cis-Cinnamic Acid Is a Novel, Natural Auxin Efflux Inhibitor That Promotes Lateral Root Formation[1][OPEN]

Ward Steenackers, Petr Klíma, Mussa Quareshy, Igor Cesarino, Robert P. Kumpf, Sander Corneillie, Pedro Araújo, Tom Viaene, Geert Goeminne, Moritz K. Nowack, Karin Ljung, Jiří Friml, Joshua J. Blakeslee, Ondřej Novák, Eva Zažímalová, Richard Napier, Wout Boerjan[2]*, and Bartel Vanholme[2]*

Department of Plant Systems Biology, VIB, B-9052 Gent, Belgium (W.S., I.C., R.P.K., S.C., P.A., T.V., G.G., M.K.N., W.B., B.V.); Department of Plant Biotechnology and Bioinformatics, Ghent University, B-9052 Gent, Belgium (W.S., I.C., R.P.K., S.C., P.A., T.V., G.G., M.K.N., W.B., B.V.); Institute of Experimental Botany, Czech Academy of Sciences, CZ-16502 Prague, Czech Republic (P.K., E.Z.); School of Life Sciences, University of Warwick, Coventry CV4 7AL, United Kingdom (M.Q., R.N.); Department of Botany, Institute of Biosciences, University of São Paulo, Butantã, São Paulo 03178-200, Brazil (I.C.); Umeå Plant Science Centre, Department of Forest Genetics and Plant Physiology, Swedish University of Agricultural Sciences, SE-901 83 Umeå, Sweden (K.L., O.N.); Institute of Science and Technology, Austria, 3400 Klosterneuburg, Austria (J.F.); Department of Horticulture and Crop Science, The Ohio State University/Ohio Agricultural Research and Development Center, Wooster, Ohio 44691 (J.J.B.); and Laboratory of Growth Regulators, Centre of the Region Haná for Biotechnological and Agricultural Research, Institute of Experimental Botany CAS and Faculty of Science of Palacký University, CZ-78371 Olomouc, Czech Republic (O.N.)

ORCID IDs: 0000-0001-5678-2919 (P.K.); 0000-0001-8115-9803 (M.Q.); 0000-0002-6789-2432 (I.C.); 0000-0002-4046-6935 (R.P.K.); 0000-0002-0337-2999 (G.G.); 0000-0003-2901-189X (K.L.); 0000-0002-8302-7596 (J.F.); 0000-0002-0605-518X (R.N.); 0000-0003-1495-510X (W.B.); 0000-0002-7214-7170 (B.V.).

Auxin steers numerous physiological processes in plants, making the tight control of its endogenous levels and spatiotemporal distribution a necessity. This regulation is achieved by different mechanisms, including auxin biosynthesis, metabolic conversions, degradation, and transport. Here, we introduce cis-cinnamic acid (*c*-CA) as a novel and unique addition to a small group of endogenous molecules affecting in planta auxin concentrations. *c-CA* is the photo-isomerization product of the phenylpropanoid pathway intermediate trans-CA (*t*-CA). When grown on *c*-CA-containing medium, an evolutionary diverse set of plant species were shown to exhibit phenotypes characteristic for high auxin levels, including inhibition of primary root growth, induction of root hairs, and promotion of adventitious and lateral rooting. By molecular docking and receptor binding assays, we showed that *c*-CA itself is neither an auxin nor an anti-auxin, and auxin profiling data revealed that *c*-CA does not significantly interfere with auxin biosynthesis. Single cell-based auxin accumulation assays showed that *c*-CA, and not *t*-CA, is a potent inhibitor of auxin efflux. Auxin signaling reporters detected changes in spatiotemporal distribution of the auxin response along the root of *c*-CA-treated plants, and long-distance auxin transport assays showed no inhibition of rootward auxin transport. Overall, these results suggest that the phenotypes of *c*-CA-treated plants are the consequence of a local change in auxin accumulation, induced by the inhibition of auxin efflux. This work reveals a novel mechanism how plants may regulate auxin levels and adds a novel, naturally occurring molecule to the chemical toolbox for the studies of auxin homeostasis.

Plant growth and development are tightly regulated by a plethora of signaling compounds, which are present within the plant at extremely low concentrations. Although the molecular working mechanism for several of these compounds has been described in detail (phytohormones, such as auxin and cytokinin, being among the best studied), for others the underlying mode of action is still unknown. Cinnamic acid (CA) is one of them, and whereas the first report on its biological activity dates back to 1935 (Haagen-Smit and Went, 1935; Hitchcock, 1935), little additional research has been performed on this compound.

CA is found in planta, both as trans (*t*)- and cis (*c*)-isomers, though not in equal concentrations (Yang et al., 1999; Yin et al., 2003). *t*-CA is synthesized through the deamination of Phe by PHE AMMONIA-LYASE, after which it is hydroxylated to *p*-coumaric acid by CINNAMIC ACID-4-HYDROXYLASE (C4H; Boerjan et al., 2003). These are the first steps of the general phenylpropanoid pathway that lead toward a plethora of secondary metabolites such as flavonoids, stilbenes, tannins, and monolignols (Vogt, 2010; Supplemental Fig. S1). Besides being a crucial intermediate of an important pathway, *t*-CA itself has also been described as a bioactive compound, though its exact activity has remained a matter of debate. Depending on the experiment, *t*-CA has been described as inactive, anta-, or agonistic to auxin or an inhibitor of polar auxin transport (Van Overbeek et al., 1951; Åberg, 1961; Letham, 1978; Liu et al., 1993). *c*-CA is a photoisomerization product of

t-CA and, in contrast to the latter, is detected only in trace amounts in plants (Yin et al., 2003; Wong et al., 2005). However, it has been suggested to have higher biological activity compared to *t*-CA (Haagen-Smit and Went, 1935). *c*-CA inhibits the gravitropic response of etiolated tomato (*Lycopersicon esculentum*) seedlings and young tomato plants (Yang et al., 1999) and promotes cell-elongation in *Pisum sativum* (Haagen-Smit and Went, 1935; Koepfli et al., 1938; Went, 1939) and epinastic curvature of tomato plants (Yang et al., 1999). Although these effects resemble, to some extent, the physiological effects caused by perturbed auxin or ethylene homeostasis, further studies claimed that the mode of action of *c*-CA might be different from that of auxin and independent of ethylene-signaling (Yang et al., 1999; Wong et al., 2005).

In addition to this inconsistent view on the physiological role of CA in plants, an adequate explanation concerning the molecular mechanism by which both isomers independently affect plant growth and development is lacking. We evaluated the working mechanism of CA and demonstrate that *t*-CA is inactive as a molecular signal, consistent with its role as a primary intermediate in the general phenylpropanoid pathway. In contrast, its *c*-isomer is biologically active and acts as a natural inhibitor of cellular auxin efflux, promoting lateral root formation.

RESULTS

CA Affects Plant Development

An evolutionary diverse set of plant species was grown on tissue culture medium supplemented with commercially available CA and analyzed for aberrant growth phenotypes. In the higher land plants tested, CA inhibited primary root growth and induced the proliferation of adventitious and lateral roots in a dose-dependent manner (Fig. 1A; Supplemental Fig. S2, A–D). In the Pteridophyte *Selaginella moellendorffii*, CA affected root apical meristem bifurcation, thickening of the root and root hair proliferation, resulting in a more dense root architecture (Supplemental Fig. S2E). In *Physcomitrella patens*, representing the Bryophytes, no clear effect on rhizoid growth was observed, but CA did stimulate cell and leaf elongation in the gametophores (Supplemental Fig. S2, F and G). These results indicate that the addition of CA to the growth medium affects plant growth and development throughout the plant lineage.

To study the underlying molecular working mechanism of this compound, we focused on Arabidopsis (*Arabidopsis thaliana*). In this model plant, the $IC_{50\text{-root}}$ value (i.e. the CA concentration needed to reduce the primary root length by 50%) was determined to be 9.2 μM under the conditions tested (Fig. 1B). Lateral root formation and adventitious rooting were stimulated, and the overall increase in number of emerged lateral roots combined with the reduction in primary root length resulted in a considerable increase in lateral root density (LRD). A 1.4- and 2.5-fold increase in LRD was obtained at applied CA concentrations of 2.5 and 5 μM, respectively (Fig. 1C). Concentrations above 10 μM resulted in the outgrowth of fasciated lateral roots along the primary root and a significant increase in the number of adventitious roots (Fig. 1, D and E). Besides, an increase in root hair number and length was observed not only on the primary root (Fig. 1F), but also on the lateral roots (Fig. 1G). Finally, a root-waving phenotype was observed in CA-treated plants (Fig. 1A), indicating gravitropism defect. This was confirmed

[1] This work has been supported by grants from the Hercules Foundation for the Synapt Q-Tof (grant no. AUGE/014), by the Multidisciplinary Research Partnership "Biotechnology for a Sustainable Economy" (01MRB510W) of Ghent University, and by the Stanford University Global Climate and Energy Project ("Lignin management: optimizing yield and composition in lignin-modified plants"); S.C. is supported by the Research Foundation Flanders for a predoctoral (3G032912) fellowship; W.S. is supported by the Agency for Innovation by Science and Technology in Flanders for a predoctoral fellowship; J.F. is supported by the European Research Council (project ERC-2011-StG-20101109-PSDP); R.P.K. acknowledges the OMICS@VIB postdoctoral program of the VIB; P.K. and E.Z. were supported by the Czech Science Foundation (project no. 16-10948S) and EU Operational Programme Prague - Competitiveness (project no. CZ.2.16/3.1.00/21519), and O.N. acknowledges the Ministry of Education, Youth and Sport of the Czech Republic (the National Program for Sustainability I, grant no. LO1204); K.L. acknowledges the Swedish Governmental Agency for Innovation Systems and the Swedish Research Council; R.N. acknowledges the support of the Biotechnology and Biological Sciences Research Council (BB/L009366); I.C. acknowledges the Foundation for Research of the State of São Paulo for the Young Investigators Awards research fellowship (grant 2015/02527-1); P.A. acknowledges Conselho Nacional de Desenvolvimento Científico e Tecnológico fellowship (201998/2011-4).

[2] These authors contributed equally to the article.

* Address correspondence to bartel.vanholme@psb.vib-ugent.be and wout.boerjan@psb.vib-ugent.be.

The author responsible for distribution of materials integral to the findings presented in this article in accordance with the policy described in the Instructions for Authors (www.plantphysiol.org) is: Bartel Vanholme (bartel.vanholme@psb.vib-ugent.be).

W.S. designed the experiments, performed most of the experiments, analyzed the data, and wrote the article; P.K. performed the auxin accumulation assays; M.Q. performed auxin-binding and anti-auxin experiments using surface plasmon resonance and did docking analysis; I.C. assisted in designing the experiments, provided technical assistance, and assisted in writing; S.C. and T.V. provided technical assistance with all experiments performed with *Physcomitrella patens*; R.P.K. and P.A. provided technical assistance with confocal imaging and diverse phenotyping experiments, respectively; G.G. provided technical assistance on ultraperformance liquid chromatography-mass spectrometry and performed data analysis; O.N. performed the auxin metabolite profiling; J.J.B. performed the rootward auxin transport assays using radiolabeled [^{3}H]IAA; K.L., E.Z., and R.N. assisted in designing the experiments and complemented the writing; M.K.N. complemented the writing; J.F. and J.J.B. contributed to the experimental design and complemented the writing; B.V. and W.B. conceived the project, assisted in designing the experiments, supervised the experiments, and wrote the article.

[OPEN] Articles can be viewed without a subscription.

www.plantphysiol.org/cgi/doi/10.1104/pp.16.00943

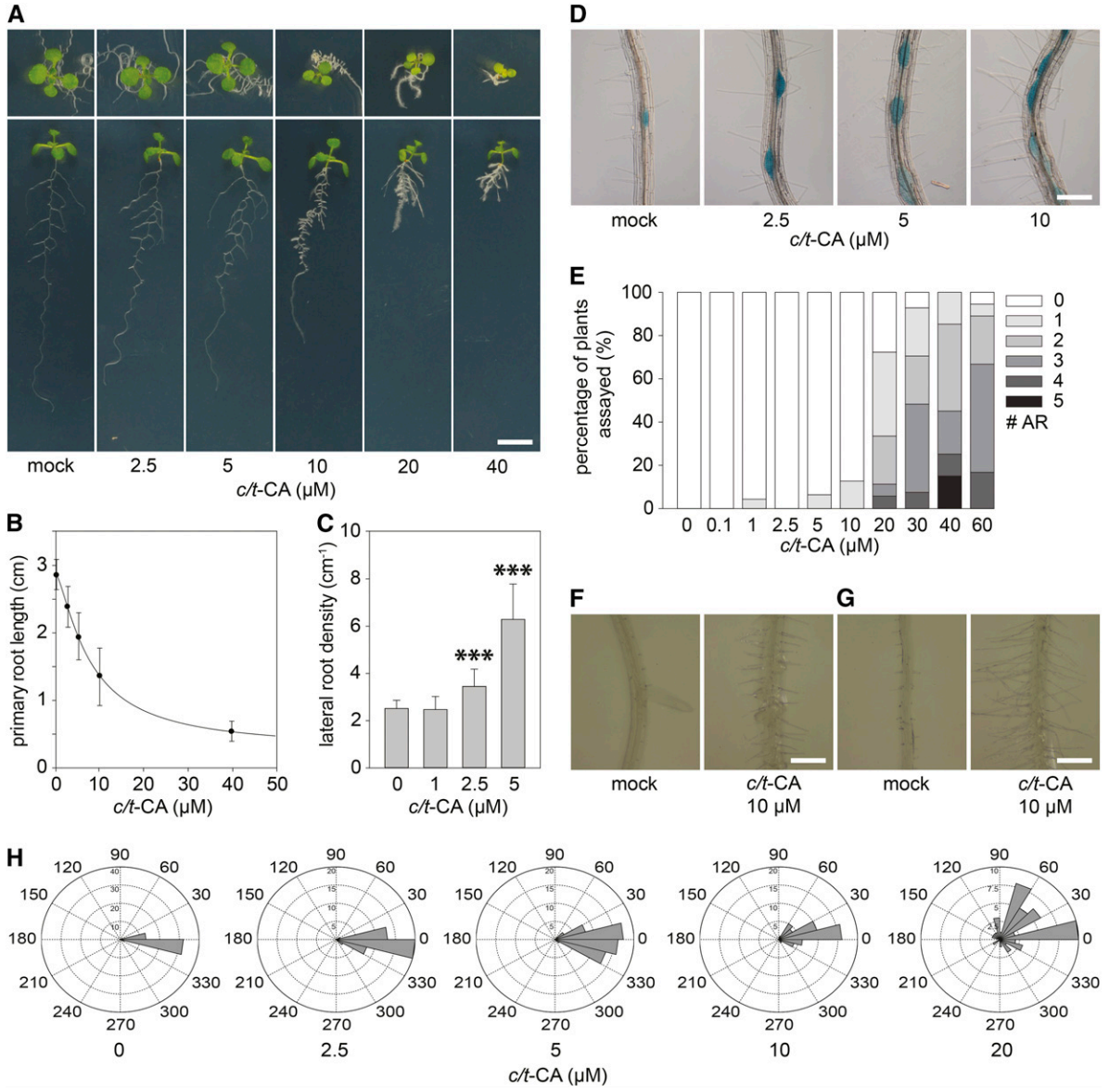

Figure 1. Effect of *c/t*-CA on growth and development of Arabidopsis. A, Root/rosette phenotype of representative seedlings 12 DAG, grown on 0.5× Murashige and Skoog medium supplemented with *c/t*-CA ($n > 20$ for each concentration; scale bar, 1 cm). B, *c/t*-CA dose response curve for primary root growth (Sigmoidal-logistic, 4 parameters; $n > 20$). Error bars represent standard deviations. C, LRD of seedlings 12 DAG, grown on 0.5× Murashige and Skoog medium supplemented with *c/t*-CA ($n > 15$). Error bars represent standard deviations and asterisks were used to indicate statistically significant differences compared to the corresponding mock-treated control sample as determined by Dunnett's test *P* values: $^{*}P < 0.05$, $^{**}P < 0.001$, $^{***}P < 0.0001$. D, Representative light microscopic images of a root segment with lateral root primordia visualized by *pCYCB1:GUS* expression in Arabidopsis 12 DAG of seedlings grown on 0.5× Murashige and Skoog medium supplemented with different concentrations of *c/t*-CA ($n > 10$; scale bar: 0.5 cm). E, Number of adventitious roots of seedlings 12 DAG grown on 0.5× Murashige and Skoog medium supplemented with *c/t*-CA. Plants were grown for 7 d in darkness (after a short light pulse of 4 h with red light to induce germination) and subsequently transferred to light to stimulate adventitious rooting. Adventitious root numbers are represented in grayscale ($n > 20$). F and G, Binocular microscopic images of a root segment of the (F) primary root and (G) lateral root of seedlings 12 DAG, grown on 0.5× Murashige and Skoog medium supplemented with 10 μM *c/t*-CA ($n = 10$). H, Histogram showing the *c/t*-CA-induced disruption of the gravitropic response in the main root. Seeds were germinated on 0.5× Murashige and Skoog medium, and 4 DAG seedlings were transferred to 0.5× Murashige and Skoog medium supplemented with *c/t*-CA. Subsequently, seedlings growing on vertical plates were rotated 90 degrees and each root was assigned to one of 12 30° sectors after 48 h incubation ($n > 25$).

in a bending assay, revealing a dose-dependent perturbation of the gravitropic response by CA (Fig. 1H).

All experiments were performed with pure *t*-CA; however, photo-isomerization toward its *c*-isomer could not be excluded during these experiments. The light-mediated isomerization of CA is well described and is induced by UV-B (Hocking et al., 1969). Although UV-B radiation (280–315 nm) was detected in the growth chamber, the intensity was low ($\sim$0.02 W/m^2) and may not have been sufficient to increase the concentration of *c*-CA in the tissue culture medium during the growth period. To determine the isomerization efficiency under the applied plant growth conditions, 2.5 mg commercially available *t*- or *c*-CA was dissolved in 50 mL Milli-Q-H_2O/dimethyl sulfoxide (DMSO; 80/20). Both solutions were subsequently placed in the growth chamber and the isomerization of both isomers was followed over time by ultra-high-pressure liquid chromatography-mass spectrometry (UHPLC-MS). The chemical equilibrium was in favor of the *c*-isomer (57%) and was reached after 8 or 15 d, depending on the use of *c*-CA or *t*-CA as the initial compound (Supplemental Fig. S3). This indicates that despite the application of *t*-CA to the growth medium, a substantial amount of the *c*-isomer could be expected during the period of plant growth. Consequently, the observed growth defects could not be linked unambiguously to the presence of *t*-CA in the medium.

No spontaneous isomerization was detected in the dark, under deep-red (650–670 nm), or far-red illumination (725–750 nm). Therefore, experiments to reveal the effect of the pure isomers could be performed under these conditions. To distinguish the experiments performed with *t*-CA in the dark from experiments performed in the light, the latter will be indicated as *t*/*c*-CA here onwards, although *t*-CA was added to the tissue culture medium for both experiments.

Knowing the photo-isomerization conditions, we questioned if both isomers had similar biochemical properties. Arabidopsis seeds were placed on 0.5× Murashige and Skoog medium supplemented with either pure *c*-CA or *t*-CA and incubated in darkness to avoid photoisomerization. Twelve days after germination (DAG) seedlings were screened for phenotypes as before. Whereas no effect on the elongation of the hypocotyl was observed (Fig. 2A), an inhibitory effect on primary root growth was evident (Fig. 2B). Here *c*-CA was much more effective than *t*-CA ($IC_{50\text{-root}}$ of 3.2 μM and 82.4 μM for *c*- and *t*-CA, respectively). To test the metabolism of *t*- versus *c*-CA, a yeast heterologous expression system was used to express Arabidopsis C4H. In contrast to *t*-CA, *c*-CA was not converted to *p*-coumaric acid by Arabidopsis C4H (Supplemental Fig. S4).

Therefore, only *t*-CA is an intermediate in the general phenylpropanoid pathway. The *c*-isomer is the biologically active isomer affecting a number of developmental processes in planta, and it is likely that most if not all physiological effects that have been previously attributed to the *t*-CA isomer or CA in general are caused by *c*-CA.

c-CA Affects Root Architecture

In Arabidopsis, lateral roots arise from asymmetric anticlinal divisions of founder cells in the pericycle layer basal to the main root meristem (De Rybel et al., 2010). As *c*-CA causes lateral root proliferation (Fig. 1D), the effect of *c*-CA on cell division in this cell layer was studied in more detail using the cell plate marker KNOLLE. An increase in the expression of *KNOLLE*-driven *GFP* was observed along the pericycle of 7-d-old dark-grown seedlings treated for 3 d with 10 μM *c*-CA, confirming strong induction of mitotic activity in this cell layer upon addition of *c*-CA (Fig. 2C). Notably, the treatment resulted in epidermal and cortical cell peeling (Fig. 2C), suggesting active degradation of the pectin-rich middle lamella between adjacent cells. POLYGALACTURONASE ABSCISSION ZONE ARABIDOPSIS THALIANA (PGAZAT)-mediated pectin degradation is known to be important for lateral root outgrowth (González-Carranza et al., 2007; Kumpf et al., 2013), and the *PGAZAT* promoter turned out to be strongly activated by 10 μM *c*-CA in cortical and epidermal cell layers surrounding developing lateral roots, but not in the lateral roots themselves (Fig. 2D). The active cell wall remodeling in the epidermis and cortex will facilitate the outgrowth of the *c*-CA-induced lateral roots.

Both the *KNOLLE* and *CYCB1* reporter lines highlighted the effect of *c*-CA on the left-right alternation and spatial organization characteristic for Arabidopsis lateral roots (Figs. 1D and 2C). The altered root pattern could originate at the level of lateral root founder cell specification, which occurs in the basal meristem before the initial anticlinal division of the founder cells (De Rybel et al., 2010). To visualize the effect of *c*-CA on lateral root priming, we used a reporter line harboring the promoter of the GATA23 transcription factor fused to a *GUS* reporter. *GATA23* expression is considered as hallmark of the earliest steps in lateral root formation (De Rybel et al., 2010). In mock-treated plants, *GUS* expression was observed in pericycle cells starting close to the root tip and continued along the root in a zone lacking emerged lateral root primordia. Treating the marker line 5 DAG with 2.5 μM *c*-CA for 21 h resulted in ectopic and enhanced GUS activity stretching continuously from the main root tip onwards till the maturation zone. In addition, local patches of strong GUS activity were observed, most likely corresponding to founder cell formation in pericycle cells adjacent to xylem pools (Fig. 2E; Supplemental Fig. S5).

These results reveal that *c*-CA triggers cell priming, which initiates lateral root proliferation. *t*-CA included in each set of experiments for comparison never induced an effect different from the mock-treatment, supporting our previous finding that the biological activity of CA is restricted to its *c*-isomer.

c-CA Triggers an Auxin Response

Lateral root proliferation is a classical auxin-mediated process. To disclose putative cross-talk between *c*-CA and auxin, we monitored whether *c*-CA

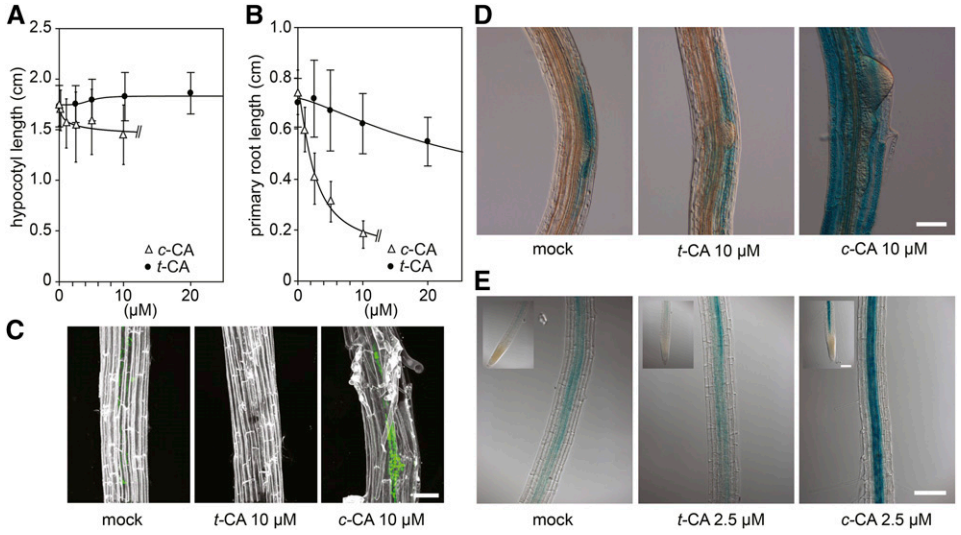

Figure 2. Effect of *c*-CA on root architecture. Dose response curves (Sigmoidal-logistic, four parameters) showing the effect of *c*-CA (triangles) or *t*-CA (dots) on (A) hypocotyl and (B) root length of seedlings 12 DAG, grown in darkness on 0.5× Murashige and Skoog medium supplemented with either *c*- or *t*-CA ($n > 20$). Seed germination was induced by a 4 h red light pulse. C, Confocal images showing *KNOLLE* promoter activity (green) of 10 DAG *pKNOLLE:KNOLLE-GFP* seedlings. D and E, Light microscopic images of *c*-CA-induced GUS activity in 10 DAG *pPGAZAT:GUS* and *pGATA23:GUS* seedlings. GUS activity was monitored at the lateral roots (PGAZAT) or the zone basal to the main root tip (GATA23; scale bar: 17.5 μm). For the *pGATA23* driven *GUS* expression the main root tip is shown as inset (scale bar: 20 μm). For C and D, seeds were germinated on 0.5× Murashige and Skoog medium and 7 DAG seedlings were transferred to 0.5× Murashige and Skoog medium supplemented with 10 μM *c*-CA or *t*-CA ($n = 5$; scale bar: 15 μm). Growth conditions for E were as for C with the only exception that *c*-CA and *t*-CA were used at 2.5 μM ($n = 5$).

could affect the local auxin response along the primary root using the auxin response reporter *pDR5:LUC* (Moreno-Risueno et al., 2010). Arabidopsis seedlings were transferred 5 DAG to 0.5× Murashige and Skoog medium supplemented with the compound of interest and luciferase activity was monitored every 10 min over a 12 h time interval. In mock-treated plants, luciferase activity was seen in the shoot/root apical meristems and lateral root initiation sites. This spatial pattern is in line with the described distribution of auxin maxima along the primary root of Arabidopsis seedlings (Benková et al., 2003). Supplying the medium with 10 μM *t*-CA did not affect this pattern, whereas the addition of 1 μM naphthalene-1-acetic acid (NAA) resulted in a strong increase in luciferase activity along the primary root from the first time point onwards, and the signal intensity increased over time (Fig. 3A; Supplemental Fig. S6). Similar to NAA, *c*-CA caused an increase in the luciferase signal in a dose-dependent manner. When supplied at 10 μM, the signal accumulated along the primary root. However, after 6 h, the luciferase activity dropped in the root maturation zone but remained in the lateral root primordia and the primary root tip, where the signal accumulated to saturation levels. This spatial distribution was highly similar to that obtained with a lower *c*-CA dose (5 μM), although the whole process was slower and never reached saturation during the time span of the experiment. (Fig. 3A; Supplemental Fig. S6).

Besides the spatial shift of the *c*-CA-induced *pDR5*-driven signal along the longitudinal axis of the root, an axial redistribution of the signal was observed as well. To follow and quantify this lateral distribution over time, we shifted to 4D microscopy using *pDR5rev:GFP* seedlings (Friml et al., 2003), grown and treated as for the *pDR5:LUC* experiment. After transferring seedlings 5 DAG to the *c*-CA-containing medium (10 μM), the region between two young emerged lateral roots was scanned every hour over a 16 h period. At the second time point (2 h), a strong increase in fluorescence was observed in the stele, increasing with time and expanding across the pericycle into neighboring cell layers (Fig. 3B; Supplemental Fig. S7). A comparable pattern was obtained with 1 μM NAA (included as positive control), although the fluorescence at the end of the observation period was lower as compared to that achieved with *c*-CA-treatment (Fig. 3B; Supplemental Fig. S7).

These observations show that *c*-CA has auxin-like effects on plant development and affects the spatial distribution of the auxin response at low micro molar concentrations.

c-CA Does Not Act as a Typical Auxin

The overall similarity in *pDR5*-driven fluorescence between *c*-CA- and NAA-treated plants suggests that *c*-CA functions via the TRANSPORT INHIBITOR RESPONSE1/AUXIN SIGNALING F-BOX (TIR1/AFB)

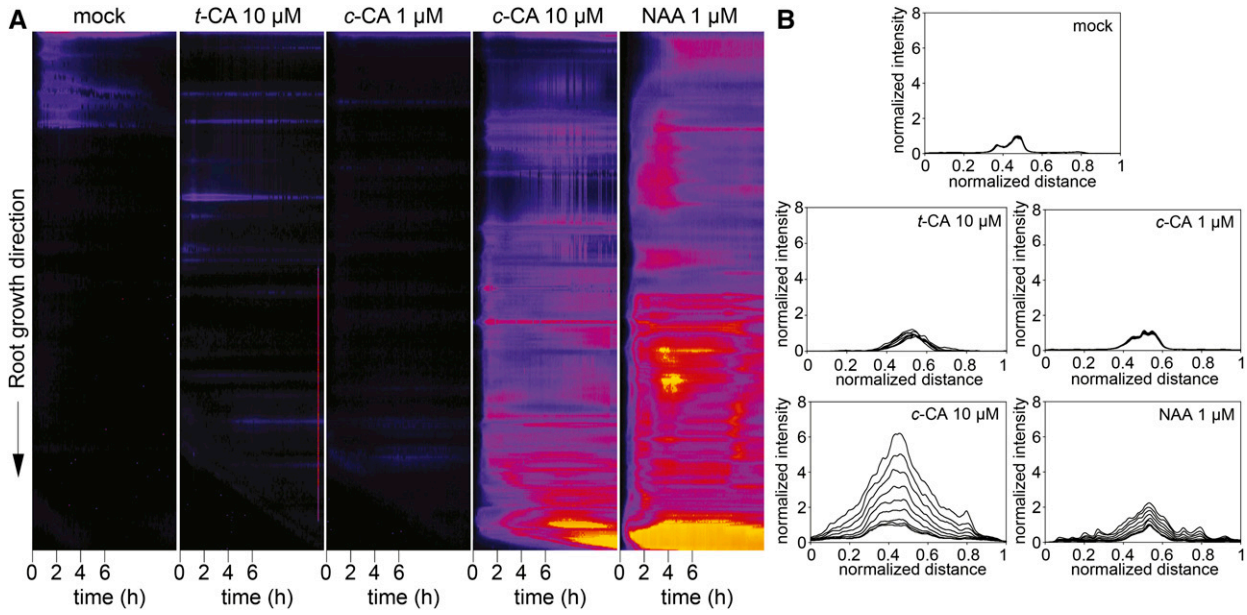

Figure 3. *c*-CA induces an auxin response in Arabidopsis. A, Kymograph of pDR5:LUC intensity along the primary root of Arabidopsis seedlings during a 12 h period. The kymograph represents on the vertical axis the primary root, with the root tip present in the origin of the coordinate system, and the shoot/root junction at the end of the vertical axis. The horizontal axis represents time. Seeds were germinated on 0.5× Murashige and Skoog medium, and 5 DAG seedlings were transferred to 0.5× Murashige and Skoog medium supplemented with 1 to 10 μM *c*-CA, 10 μM *t*-CA, or 1 μM NAA. Imaging was started at the moment of transfer and data were recorded every 10 min. Each kymograph represents one experiment. The kymograph is representative for eight biological repeats (seedlings). B, Confocal time-lapse imaging of pDR5rev:GFP intensity in the primary root between two young emerged lateral roots. At the start of the time lapse, seedlings were placed in glass-bottomed dishes and covered with 0.5× Murashige and Skoog medium containing 1 μM NAA, 1 to 10 μM *c*-CA, or 10 μM *t*-CA. The time lapse was started 5 min after the seedlings had been placed in contact with the media and captured every 60 min over a 16 h period. Cumulative spectra were obtained by projecting the GFP intensity on a virtual line crossing the middle of the primary root. Normalization was performed against the maximal intensity of the signal at the earliest time point (n = 1). Each spectrum is representative for three biological repeats (positions along the primary root).

auxin-signaling pathway (Péret et al., 2009). To investigate whether *c*-CA acts via this canonical auxin-signaling pathway, we grew the *solitary root1* (*slr*) gain-of-function Aux/indole-3-acetic acid (IAA) mutant and the *arf7 arf19* double mutant on *c/t*-CA-supplemented medium. Like auxin, *c/t*-CA failed to induce lateral root formation in these mutants, suggesting that *c*-CA functions upstream of these steps in the auxin signaling cascade toward lateral root formation (Fig. 4A). As SLR1/IAA14 is a direct target of the auxin receptor TIR1, we subsequently tested whether TIR1 was essential for *c*-CA activity by growing the *tir1 afb2 afb3* mutant on *c/t*-CA-containing medium. As for the other mutants tested, no lateral roots were induced in this mutant, indicating that the TIR1 auxin receptor is crucial for this *c*-CA-mediated growth defect (Fig. 4A). Based on these observations, we concluded that *c*-CA could be an auxin analog that induces the auxin signaling cascade by interacting with the TIR1 auxin receptor in a similar way as the native auxin, IAA. However, simulation of the molecular docking of *c*-CA in the auxin receptor pocket of TIR1 revealed a position different from the experimentally determined orientation of IAA (Supplemental Fig. S8). To validate the prediction, the interaction kinetics of TIR1 and the related AFB5 with immobilized peptides corresponding to the degron motif of Aux/IAA7 were followed using surface plasmon resonance (SPR). Whereas strong signals were obtained with IAA and NAA used as a positive controls, no evidence for a specific binding of *c*-CA or *t*-CA to the auxin receptors was found (Fig. 4B). Both isomers were also tested for anti-auxin activity. Although such property was claimed for *t*-CA (Van Overbeek et al., 1951), no supporting evidence for such activity was found (Fig. 4B).

Together, these results indicate that neither CA-isomer acts as an auxin agonist nor an antagonist at the level of the auxin perception and support the hypothesis that *c*-CA acts via an auxin-dependent pathway for lateral root formation by modifying auxin homeostasis or the spatiotemporal distribution of auxin in roots.

c-CA Triggers Lateral Root Formation in an Auxin-Dependent Manner

To assess whether activation of the *DR5* promoter is due to an overall shift in IAA concentrations, UHPLC-MS profiling was performed on Arabidopsis

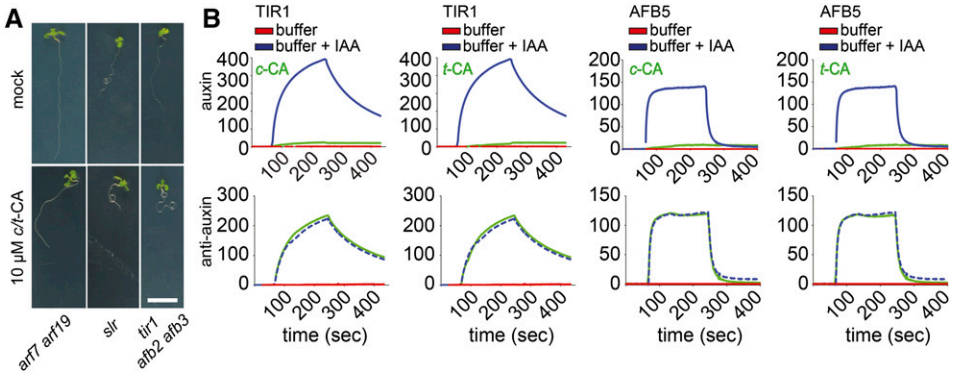

Figure 4. *c*-CA does not act as a typical auxin. A, Root phenotype of *arf7 arf19, slr,* and *tir1 afb2 afb3* mutants 12 DAG, growing on 0.5× Murashige and Skoog medium supplemented with 10 μM *c*/*t*-CA ($n > 25$; scale bar, 1 cm). B, SPR sensorgrams showing the auxin-dependent interaction between TIR1 or AFB5 with IAA DII. Each sensorgram shows the binding with IAA (blue), an auxin-free injection (red), plus the data for each test compound (green). For auxin activity assays (top), compounds (50 μM) were mixed with TIR1 or AFB5 prior to injection over DII peptide. For anti-auxin assays (bottom), compounds (50 μM) were mixed with TIR1 or AFB5 plus 5 μM IAA prior to injection. The degron sequence that was used is biot-AKAQVVGWPPVRNYRKN.

seedlings 12 DAG. Before the extraction plants were treated with 10 μM *c*-CA or *t*-CA for 1 and 6 h (Supplemental Figs. S9 and S10). No major shifts in the IAA metabolome were observed between *t*-CA- and mock-treated plants again confirming the absence of bioactivity for this compound. For the *c*-CA-treatment, an effect was observed 6 h after the transfer of the seedlings to 10 μM *c*-CA (Supplemental Fig. S10). At this point a small but significant increase in indole-3-acetamide, indole-3-acetonitrile, and indole-3-acetaldoxime was observed. In addition, intermediates of the indole-3-pyruvic acid pathway for IAA biosynthesis accumulated in seedlings treated with *c*-CA for 6 h. This pattern could be transient, as no significant increase in free IAA levels or in any of its conjugates was detected after 6 h. The absence of a clear shift in free IAA levels in combination with the observed rapid and strong activation of the *DR5* promoter questions the importance of auxin biosynthesis for *c*-CA-induced lateral root formation. The role of IAA itself was reconsidered by testing lateral root induction in plants with artificially reduced IAA levels using the IAA Lys synthase (iaaL) overexpressing line. The bacterial *IAAL* gene encodes an enzyme that inactivates IAA by conjugating it to the amino acid Lys. Seeds from the *p*35S:*iaaL*-line were germinated as above, and LRD was quantified 12 DAG. When treated with *t*/*c*-CA, *p*35S:*iaaL* plants showed fewer lateral roots than wild-type plants, indicating that *c*-CA-induced lateral root induction is indeed mediated by free IAA (Supplemental Fig. S11).

In summary, the bioactivity of *c*-CA is clearly dependent on auxin. The fact that free IAA is not increased in *c*-CA-treated plants suggests that auxin is redistributed within the plant, resulting in novel auxin maxima that inhibit primary root growth and promote lateral root development.

c-CA Inhibits Cellular Auxin Efflux

The ability of *c*-CA to induce an auxin response via the canonical auxin-signaling pathway without being a receptor agonist suggests that *c*-CA interferes with tightly controlled auxin concentrations in the plant. To obtain insight into possible *c*-CA-mediated dynamic changes of auxin responses at high spatial resolution in a short time-interval, the visual marker DII-VENUS was used (Brunoud et al., 2012). A time course was recorded of DII-VENUS fluorescence in the primary root tip of Arabidopsis seedlings 7 DAG. Forty-five minutes after the addition of 1 μM NAA DII-VENUS fluorescence dropped to 25% of its initial intensity (Fig. 5A; Supplemental Fig; S12), which is in line with previously published data (Brunoud et al., 2012). The DII-VENUS sensor reacted in a similar way following treatment with *c*-CA, although compared to NAA, a 10-fold higher concentration of *c*-CA was required to reduce the fluorescence to a comparable level (i.e. 29% of the initial fluorescence after 42 min with 10 μM *c*-CA; Fig. 5A and Supplemental Fig. S12). Remarkably, also *t*-CA turned out to be active in this assay, which contradicts previous findings claiming activity restricted to the cis-isoform. However, the *t*-CA-mediated reduction of DII-VENUS signal is most likely a direct consequence of laser-mediated isomerization of *t*-CA toward *c*-CA during imaging (so called photo-activation). Lowering the concentration of *c*-CA to 1 μM resulted in a pattern indistinguishable from that of mock-treated samples during the initial time points. Intriguingly, after 10 min, the pattern started to deviate from the negative control, and a slight increase in DII-VENUS degradation could be observed. This trend was sustained and resulted in a significant drop in fluorescence by the end of the experiment. Interestingly, DII-VENUS degraded at a similar speed as in the samples treated with the higher concentration of *c*-CA (Fig. 5A). This peculiar profile could indicate that *c*-CA interferes with auxin

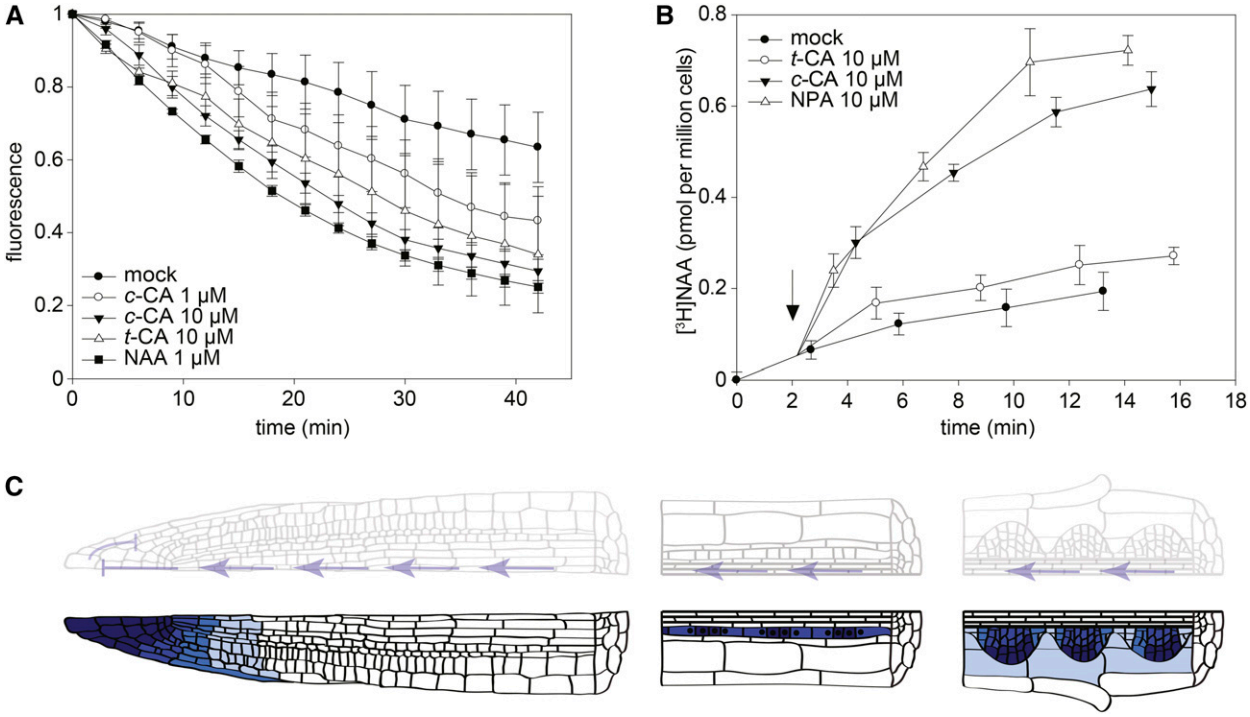

Figure 5. Effect of *c*-CA on polar auxin transport. A, Time course of DII-VENUS fluorescence in the main root tip of DII-VENUS-YFP seedlings. Plants were germinated on 0.5× Murashige and Skoog medium and subsequently transferred 5 DAG to 0.5× Murashige and Skoog medium supplemented with 1 or 10 μM *c*-CA, 10 μM *t*-CA, or 1 μM 1 NAA (n = 3; scale bar: 50 μm). Fluorescence was quantified every 3 min over a 42 min period. During each experiment, three root tips (representing one treatment) were simultaneously imaged. Error bars represent standard deviations. B, Effect of 10 μM *c*-CA, *t*-CA, or NPA on the net accumulation of [^{3}H]NAA in 2-d-old suspension-cultured tobacco BY-2 cells (20 min uptake period). The arrows points to the time of application of the compound. Error bars represent standard deviations (n = 4). C, Model explaining the *c*-CA-mediated lateral root proliferation. *c*-CA inhibits shootward auxin transport by inhibiting the redistribution of auxin in the meristem. This is considered a direct consequence of the *c*-CA-mediated inhibition of auxin efflux. The phloem-mediated rootward auxin transport in the primary root is not disturbed by *c*-CA, allowing a continuous supply of auxin from the shoot toward the root tip. The block of a proper auxin redistribution in the meristem results in the accumulation of auxin in the primary root, where it triggers lateral root proliferation. Top, Auxin flow (blue arrows) and its perturbation within the primary root of *c*-CA treated plants. Bottom, Schematic representation of auxin accumulation in the primary root of *c*-CA treated plants and the consequent induction of lateral roots (model based on De Rybel et al., 2010).

transport. This would lead to increasing intracellular auxin concentrations and consequent DII-VENUS degradation once a critical auxin concentration threshold is passed. To find supporting evidence for this hypothesis, the experiment was repeated with 1-naphthylphthalamic acid (NPA), a well-established inhibitor of auxin efflux. As for *c*-CA, NPA caused a dose-dependent reduction in DII-VENUS fluorescence with similar dynamics as after treatment with *c*-CA, indicating that both these compounds similarly increase auxin accumulation in the primary root tip (Supplemental Fig. S13). In line with the proposed model, at the lower concentrations tested (0.1 and 1.0 μM NPA), a pattern was obtained that only deviated from the mock-treated control after a temporal delay, of which the length was dependent on the NPA concentration (Supplemental Fig. S13).

The putative link between *c*-CA and polar auxin transport machinery was further explored by auxin accumulation assays on the cellular level. Polar auxin transport depends on the localization and activity of auxin influx and efflux carriers (Adamowski and Friml, 2015). In tobacco (*Nicotiana tabacum*) cells, NAA enters the cells mainly by diffusion (Delbarre et al., 1996; Seifertová et al., 2014), whereas it is an excellent substrate for active efflux. Therefore, a change in intracellular accumulation of radioactively labeled NAA in BY-2 tobacco cell-suspension cultures over time provides a measure of the activity of auxin efflux from cells (Fig. 5B). Control cells displayed [^{3}H]NAA accumulation kinetics indicative of active and saturable auxin-efflux (Petrášek et al., 2006). After treatment with NPA, [^{3}H]NAA accumulated strongly inside the cells, and a similar although slightly reduced response was obtained when NPA was replaced with *c*-CA, indicating that *c*-CA acts as a potent inhibitor of auxin efflux. This increase in accumulation was not observed upon treatment with *t*-CA (Fig. 5B). When a similar experiment was performed with a combination of NPA and *c*-CA, [^{3}H]NAA accumulated to a similar level as in NPA-treated cells, indicating *c*-CA targets a subset of NPA-sensitive auxin transporters

(Supplemental Fig. S14), which could be either PIN-FORMED (PIN) or ATP-binding cassette-B (ABCB) transporters (Petrášek and Friml, 2009). To distinguish between both, NPA was substituted for the ABCB-specific inhibitor 2-[4-(diethylamino)-2-hydroxybenzoyl] benzoic acid (BUM; Kim et al., 2010). In contrast to NPA, BUM inhibited auxin efflux to the same extent as *c*-CA in the auxin transport assay, and no additive effect was observed when BUM and *c*-CA were used simultaneously (Supplemental Fig. S15). This strongly suggests *c*-CA targets predominantly the ABCB-auxin transport machinery. To test whether *c*-CA might also affect auxin influx, [^{3}H]NAA was replaced for [^{3}H]2,4-dichlorophenoxyacetic acid ([^{3}H]2,4-D), which is a preferred substrate for influx activity. When added to the BY-2 cell suspension, [^{3}H]2,4-D accumulated in the cells until a plateau was reached, representing equilibrium between cellular influx and efflux of the labeled compound (Supplemental Fig. S16). Using this experimental setup, we found no indication that either *c*-CA or *t*-CA affects cellular auxin influx.

Based on these experiments, we concluded that *c*-CA, but not *t*-CA, inhibits auxin efflux from cells, more specifically the ABCB-mediated part of auxin efflux. The consequent accumulation of intracellular auxin could be at the basis of the physiological and developmental defects observed in *c*-CA-treated Arabidopsis seedlings.

c-CA Does Not Inhibit Long-Distance Rootward Auxin Transport

Although both NPA and *c*-CA block cellular auxin efflux, their effects on Arabidopsis roots are entirely different. NPA arrests (Casimero et al., 2001; Benková et al., 2003) and *c*-CA induces lateral root formation. Supported by the spatiotemporal distribution of *pDR5*-driven luciferase activity, we hypothesized that a difference in long-distance auxin transport could be the origin of the phenotypic difference between these two auxin efflux inhibitors. Whereas NPA affects both rootward and shootward auxin transport in the primary root (Casimero et al., 2001), the strong increase in luciferase activity in the tip of *c*-CA-treated roots suggested that rootward auxin transport is not disturbed by *c*-CA. To verify this hypothesis, we monitored whether local *c*-CA application could affect distant auxin-inducible luciferase activity using a split medium approach as described by Lewis and Muday (2009). To this end, seedlings were positioned on the medium in a way that either the upper or the lower half of the root was in contact with *c*-CA. Dynamics of luciferase activity along the root were followed over time as described above. When the lower half of the root was in contact with *c*-CA, luciferase activity accumulated in the root tip in line with earlier data (Supplemental Fig. S17). When only the upper part of the root was in contact with *c*-CA, the luciferase signal quickly extended toward the non-treated zone (Supplemental Fig. S17). This illustrates that auxin appears to be able to pass through the *c*-CA-treated zone in a rootward direction.

Although the data support the hypothesis that *c*-CA allows long-distance rootward auxin transport, we could not exclude an alternative explanation, namely that *c*-CA itself is transported and triggers auxin signaling locally. To provide undisputed evidence for rootward transport of auxin in *c*-CA-treated roots, long-distance rootward auxin transport was assayed in primary roots of Arabidopsis seedlings in which the roots were exposed to either mock or *c*-CA-treated 0.5× Murashige and Skoog medium. In these assays, microdroplets of radiolabeled [^{3}H]IAA were placed precisely on the shoot apical meristems of Arabidopsis seedlings, and rootward auxin transport was measured by harvesting a 4 mm segment centered on the root/shoot transition zone, as well as the entire root, in 2 mm segments. Consistent with previous results, treatment with *c*-CA did not inhibit rootward auxin movement (Fig. 5C; Supplemental Fig. S18). The strong accumulation of the auxin-inducible luciferase in the root tip is characteristic of the inhibition of shootward auxin transport (Fig. 3A; Supplemental Figs. S6 and S17). Unfortunately, reliable data were not obtained for shootward auxin transport to support this hypothesis.

Taken together, our data supports a model (Fig. 5C) in which *c*-CA inhibits auxin efflux at the cellular level in specific cells at or near the root apical meristem, while allowing long-distance rootward auxin transport at the organ level. The resultant accumulation of auxin in the root apical meristem might cause, at least in part, the observed growth defects induced by *c*-CA.

DISCUSSION

Being sessile organisms, plants cannot escape unfavorable growth conditions. This shortcoming is compensated by an extreme plasticity, allowing them to react to changing environmental cues. Here, the phytohormone auxin has an important function, as it is key in the regulation of many processes involved in growth and development (Vanneste and Friml, 2009). As for all bioactive compounds, tight regulation of its homeostasis and spatiotemporal distribution inside the plant is crucial, as suboptimal auxin concentrations will not trigger the desired response, while high concentrations will be harmful. The ability to control auxin levels is a necessity for plant survival and occurs at the cellular level by regulating biosynthesis, metabolic conversions as well as degradation, whereas transport is essential to translocate auxin between different cells and tissues. Synthetic inhibitors of auxin transport such as NPA and BUM have proven the importance of this process in diverse physiological actions, including embryogenesis, tropisms, vascular patterning, and lateral root initiation (Kim et al., 2010). Intriguingly, endogenous auxin transport inhibitors are scarce. Flavonols and flavonoids such as quercetin were considered to inhibit auxin transporters (Brown et al., 2001), although later

work suggested that flavonoids also act by redirecting PIN efflux protein localization (Santelia et al., 2008). Certain flavonoid mutants display auxin-related defects (Buer et al., 2013) and an auxin-transport inhibiting activity was recently assigned to the flavonol glycoside kaempferol 3-*O*-rhamnoside-7-*O*-rhamnoside (Yin et al., 2014).

Here, we introduce *c*-CA as a novel endogenous inhibitor of auxin transport. Intriguingly, the activity of *c*-CA resembles that of NPA, but only at the cellular level. Although both NPA and *c*-CA block cellular auxin efflux, the effects of the two compounds on Arabidopsis root architecture are entirely different, with *c*-CA inducing lateral root formation and NPA impacting lateral root initiation. The exact mechanism of NPA action is still unknown, but according to one hypothesis the *slr* phenotype of NPA-treated plants is a consequence of auxin depletion in the root due to the perturbation of basipetal and acropetal auxin transport (i.e. shootward and rootward, respectively; Casimiro et al., 2001). Although explaining the observed phenotype, the molecular mechanism underlying the inhibition of phloem-based (and hence no-transporter-mediated) rootward auxin transport by an auxin efflux inhibitor remains unknown. Proceeding from this model, we hypothesized that a difference at the level of rootward transport (perturbed by NPA but not by *c*-CA) underlies the phenotypic differences caused by the two compounds. Under mock conditions, auxin is redistributed in the root tip according to the "reverse-fountain" model, in which specific auxin transport proteins (PINs and ABCB proteins) play distinct roles in establishing directional movement of auxin (Benková et al., 2003; Blilou et al., 2005; Lewis and Muday, 2009). By inhibiting cellular auxin efflux, we hypothesize *c*-CA will affect the auxin reflux in the meristem, resulting in the inhibition of shootward auxin transport. Consequently, auxin either transported from the shoot or synthesized in the primary root tip will accumulate behind the root tip where it will trigger GATA23-expression and affect lateral root founder cell specification. Over time, the accumulating auxin will enter pericycle cells, either by diffusion or active influx where it will be trapped due to the *c*-CA-mediated inhibition of auxin efflux, similar to the situation in the primary root. Once the auxin concentration passes a critical threshold, primed cells will be triggered to develop into lateral root founder cells, which eventually will develop into new lateral roots, shaping the altered root architecture (Fig. 5C).

Compared to NPA, *c*-CA was found slightly less efficient in the auxin accumulation assay. This difference may result from the broader specificity of NPA, known to affect different types of auxin efflux carriers. Based on the absence of an additive effect of *c*-CA and BUM in this assay, we concluded that *c*-CA targets the ABCB subfamily of the multidrug-resistant/P-glycoprotein integral membrane proteins. These transporters are well known for their capacity to pump drugs out of the cell (Kang et al., 2011), increasing the resistance of the cell and hence the organism toward compounds that are considered toxic under normal conditions. Interestingly, and in line with our observation, the cis-form of CA and not its trans-form raises a notable synergistic bactericidal activity against multiple-drug-resistant *Mycobacterium tuberculosis*. It is tempting to speculate that also in this case *c*-CA blocks the MDR-transporters, resulting in the intracellular accumulation of the supplied antibiotics to levels required to kill the bacteria (Chen et al., 2011).

Although the physiological role of endogenous *c*-CA is still unclear, the beauty of this bioactive molecule lies in the fact that it can be produced from a readily available inactive compound (*t*-CA) by sunlight (Ding et al., 2011). This gives a tremendous opportunity to link environmental conditions directly to developmental regulation without the need to activate gene expression to alter the auxin pool. In addition, we cannot exclude that a similar conversion can be obtained by a yet-to-be-discovered enzyme, further extending the possibilities to exploit this mechanism to steer plant development independently of light. The question of whether *c*-CA has an active role in the regulation of plant development remains an open and intriguing question; however, the fact that it was previously found in small but physiologically relevant quantities in plants and that the effects on roots are evolutionary conserved only feeds the speculation on its importance as an endogenous plant growth regulator (Yin et al., 2003; Wong et al., 2005). This function could be different from lateral root development, a system that we only used to elucidate the molecular mechanism of *c*-CA action.

MATERIALS AND METHODS

Plant Material, Transgenic Lines, Chemicals, and Growth Conditions

The effect of *c*/*t*-CA on plant growth and development was studied in a diverse set of plant species, comprising *Physcomitrella patens*, *Selaginella moellendorffii*, *Oryza sativa*, *Nicotiana benthamiana*, *Brachypodium distachyon*, and *Arabidopsis thaliana*. Arabidopsis ecotype Columbia (Col-0) was used, unless stated elsewhere. Following transgenic lines were in the same ecotype: *DII-VENUS*, *pDR5rev:GFP*, *pDR5:LUC*, *pGATA23:GUS*, *pGAZAT:GUS*, *pKNOLLE:KNOLLE-GFP*, *p35S:iaaL*, *slr*, *arf7 arf19*, and *tir1 afb2 afb3* (Romano et al., 1991; Lukowitz et al., 1996; Fukaki et al., 2002; Friml et al., 2003; Dharmasiri et al., 2005; González-Carranza et al., 2007; Okushima et al., 2007; De Rybel et al., 2010; Moreno-Risueno et al., 2010; Brunoud et al., 2012). The transgenic line *pCYCB1:GUS* was in the ecotype Landsberg erecta (Ler; Colón-Carmona et al., 1999). Seeds were vapor-phase sterilized and grown on 0.5× Murashige and Skoog medium. The 0.5× Murashige and Skoog medium (pH 5.7) contains per liter 1.5 g Murashige and Skoog basal salt mixture powder (Duchefa), 7.14 g Suc, 0.36 g MES monohydrate, 8 g plant tissue culture agar. The medium was supplemented with one of the following compounds: NAA (Sigma Aldrich), NPA (Sigma Aldrich), *c*-CA (Shanghai Specbiochem), and *t*-CA (Sigma Aldrich) from stock solutions in DMSO (final 0.1% DMSO) to the autoclaved medium prior to pouring the plates. After sowing, seeds were incubated at 4°C for at least 2 d, whereupon plates were placed in a vertical orientation in the tissue culture chamber room under a 16-h-light/8-h-dark photoperiod at 21°C, except for the experiments done to reveal the pure *c*-CA and/or *t*-CA effect. Seedlings grown in darkness received a short 4 h red light pulse to induce germination. Propidium-iodide (PI; Sigma Aldrich) was used to counterstain the cell wall. The adventitious rooting assay was performed by placing plates in darkness for 7 d (after a short light pulse with red light of 4 h). Plates were then exposed to light for 5 d. The root-bending assay was performed

on 5-d-old seedlings treated with different concentrations of *c*/*t*-CA. After 5 d plates were rotated 90 degrees and root gravitropism was scored after 48 h. Scans were made and the quantification of the response was performed with ImageJ. Tobacco (*Nicotiana tabacum* 'Bright Yellow-2') cells of the cell line BY-2 (Nagata et al., 1992) were cultivated according to Petrášek et al. (2006) and subcultured weekly. Bromophenol blue (Sigma-Aldrich) was used to stain the cell wall of *Physcomitrella patens* leaves.

Description of Plant Phenotype

To quantify growth parameters and check for aberrant phenotypes, seeds were grown on square plates placed in a vertical orientation in the growth chamber. Plates were scanned using the Scanmaker 9800XL, and root length was measured using the ImageJ software. For each compound, the inhibitory concentration (IC_{50}) was calculated, plotting a dose-response curve in SigmaPlot. The dose-response curve resulting in the highest R^2 value (coefficient of determination) was used. The number of plants used and the timing of the scanning depends on the plant species and the treatment. The number of adventitious roots (above the root-shoot junction) and number of emerged lateral roots were counted using a stereomicroscope (CETI Binocular Zoom Stereo).

Histochemical Analysis and Confocal Microscopy

Root cell walls were stained with 30 μM PI for *pKNOLLE:KNOLLE-GFP* at the onset of the experiment. The excitation energy of 488 nm was from an argon laser. The PI fluorescence emission was collected between 550 and 650 nm and GFP/YFP between 500 and 550 nm. All images were captured with an inverted LSM 710 META confocal microscope equipped with 20×-Air objectives (Carl Zeiss). GUS assays were performed and inspected using differential interference contrast optics as described earlier in Beeckman and Engler (1994).

Time Lapse DII-VENUS

For analysis of chemically treated roots, 7-d-old DII-VENUS Arabidopsis seedlings were used. At the onset of the time lapse, three seedlings (biological repeats) were placed in glass-bottomed dishes and covered with 0.5× MS-media containing NAA, NPA, *c*-CA, or *t*-CA. The time-lapse was started 5 min after the seedlings had been placed in contact with the media and captured over 42 min (every 3 min) with an inverted LSM 710 META confocal microscope equipped with 20×-Air objectives (Carl Zeiss). Images were analyzed with the Fiji software using the total signal from Z-projection of defined region (always the same area). Normalization was done by using the initial signal from the Z-projection of adefined region as the baseline.

Time Lapse *pDR5rev:GFP*

Seven-day-old Arabidopsis seedlings were used to analyze the effect of *c*-CA, *t*-CA, NPA, and NAA on the expression of *pDR5rev:GFP* in the region between two emerged lateral roots. At the start of the time lapse, seedlings were placed in glass-bottomed dishes and covered with media containing NAA, *c*-CA, or *t*-CA. The time lapse was started 5 min after the seedlings had been placed in contact with the media and captured over a period of 16h, every hour with an inverted LSM 710 META confocal microscope (Carl Zeiss) equipped with 20×-air objective (Carl Zeiss). Images were analyzed with the Volocity software. The accumulation projection spectrum was obtained by projecting the GFP intensity on a virtual line crossing the middle of the primary root over the imaged distance of the root. This way *pDR5rev:GFP* expression can be imaged and quantified in every cell type. Normalization was performed against the intensity to the highest obtained signal at the earliest time point.

Time Lapse *pDR5:LUC*

The *pDR5:LUC* images were taken by a Lumazone machine carrying a CCD (CCD) camera (Princeton Instruments). The CCD camera that is controlled by a WinView/32 software took movies of the *LUC* expression automatically every 10 min (exposure time, 10 min) for 12 h. Before imaging, plates containing 0.5× Murashige and Skoog medium were sprayed with 1 mM D-luciferin solution (Duchefa Biochemie). The picture series were saved as TIFF format for further analysis. The luciferase signals were quantified by the measure of the analog-digital units per pixel by means of ImageJ. To visualize the spatiotemporal luciferase changes during treatment with the compound, a Kymograph (http://www.embl.de/eamnet/html/body_kymograph.html) was generated with ImageJ.

Heterologous Expression of *C4H* and Microsome Assay

The *Saccharomyces cerevisiae* strain containing the Arabidopsis *C4H* was used (Van de Wouwer et al., 2016). One hundred microliters of recombinant yeast in glycerol was grown overnight at 30°C in 5 mL liquid DO medium (Clontech Laboratories). The yeast cells were pelleted (1 min at 4000 rpm), washed with 5 mL sterile MQ water, pelleted again, and resuspended in another 5 mL water. The amount of inoculum was calculated to reach an OD600 of 0.1 and subsequently, the yeast cultures were grown for 16 h at 30°C with shaking (200 rpm) in DO medium (Clontech Laboratories) containing Gal to induce transcription. Microsomes were prepared according to Schalk et al. (1998). The microsome assay was done with aliquots of 10 μL microsome, by adding 20 mM sodium phosphate buffer (pH 7.4), 10 μL of the desired compound at final concentrations of 10 μM for *c*-CA and *t*-CA and equal amounts of DMSO as a control. To start the reaction, 10 μL of the 10 mM $NADP^+$ sodium phosphate buffer solution was added to the Eppendorf, briefly vortexed and immediately placed in the Eppendorf thermomixer at 28°C for 20 min. The reaction was stopped by adding 150 μL ice-cold methanol. The pellet was resuspended in 500 μL 90% methanol and incubated in an Eppendorf thermomixer at 30°C for 10 min while shaking at 1000 rpm. After centrifugation at 14,000 rpm for 5 min, the supernatant was transferred to a new Eppendorf tube and lyophilized. The pellet was treated with 100 μL water and 100 μL cyclohexane. After 10 min of centrifugation (14,000 rpm), 80 μL of the aqueous phase was retained for UHPLC-MS analysis. For reversed-phase LC, 10 μL of the aqueous phase was subjected to UHPLC-MS on a Waters Acquity system (Waters Corporation) connected to a Thermo LTQ XL mass spectrometer (Thermo Scientific). Chromatographic gradient separation was carried out as described in the next paragraph. The eluent was directed to the mass spectrometer via electrospray ionization in negative mode. MS source parameters were as follows: capillary temperature, 300°C; capillary voltage, 24 V; source voltage, 3.5 V; source current, 100 A; sheath gas flow, 30; aux gas flow, 20; sweep gas flow, 5. The mass range was set between 100 and 1000 D. *c*-CA, *t*-CA, and *p*-coumaric acid were characterized based on the similarity of their masses and retention times with those of standards. Peak detection and integration was done with Progenesis QI v2.1 (Nonlinear Dynamics, a Waters Company). Product/substrate ratios were calculated and *P* values were calculated using unpaired Student's *t*-tests.

LC-MS/MS and LC-UV-Vis-MS to Determine *c*- and *t*-CA Photo-Isomerization

Exactly 2.5 mg of pure *t*-CA and *c*-CA was dissolved in 50.0 mL Milli-Q-H_2O/DMSO (80/20). Solutions were subsequently incubated in the growth chamber and isomerization of both isomers was followed over time by LC-MS/MS. For darkness, plates were covered with aluminum foil to exclude light, and sampling was performed in darkness. Deep-red and far-red illumination was provided by the GreenPower LED module (Philips).

For quantification of *t*-CA and *c*-CA, a 15 μL aliquot was subjected to LC-MS analysis performed on a Waters Acquity UPLC system equipped with a PDA detector (lambda range from 190 to 500 nm; Waters Corporation) connected to a Synapt HDMS quadrupole time-of-flight mass spectrometer (Waters MS Technologies). Chromatographic separation was performed on an Acquity UPLC BEH C18 column (2.1 mm × 150 mm, 1.7 μm; Waters Corporation) using a water-acetonitrile gradient elution. Mobile phases were composed of (A) water containing 1% acetonitrile and 0.1% formic acid and (B) acetonitrile containing 1% water and 0.1% formic acid. The column temperature was maintained at 40°C, and the autosampler temperature was maintained at 10°C. A flow rate of 350 μL/min was applied during the gradient elution, with initialization at time 0 min 5% (B), 30 min 50% (B), and 33 min 100% (B). For UV-Vis detection, data were recorded between 210 and 500 nm. The eluant was then directed to the mass spectrometer equipped with an electrospray ionization source and lockspray interface for accurate mass measurements. The MS source parameters were as follows: capillary voltage, 2.5 kV; sampling cone, 37 V; extraction cone, 3.5 V; source temperature, 120°C; desolvation temperature, 400°C; cone gas flow, 50 L h^{-1}; and desolvation gas flow, 550 L h^{-1}. The collision energy for the trap and transfer cells was 6 and 4 V, respectively. For data acquisition, the dynamic range enhancement mode was activated. Full-scan data were recorded in negative centroid V-mode; the mass range between *m/z* 100 and 1000, with a scan speed of 0.2 s $scan^{-1}$. Leucin-enkephalin (250 pg μL^{-1}; solubilized in water: acetonitrile 1:1 [v/v] with 0.1% [v/v] formic acid) was used for

lock mass calibration, with scanning every 10 s with a scan time of 0.5 s. All data were recorded with Masslynx software (version 4.1, Waters). For the quantification of *t*-CA and *c*-CA, the UV-Vis chromatogram was extracted at 277 nm, and peaks were integrated automatically (automatic noise measurement; mean smoothing [window size, 3; no. of smooths, 2]). Peak areas were used to calculate the conversion of *t*-CA and *c*-CA.

Auxin Metabolite Profiling

Extraction and purification of auxin and its metabolites was done as described previously with minor modifications (Novák et al., 2012). Frozen samples were homogenized using a MixerMill (Retsch GmbH) and extracted in 1 mL 50 mM sodium phosphate buffer (pH 7.0) containing antioxidant (1% sodium diethyldithiocarbamate) and a cocktail of deuterium and $^{13}C_6$-labeled internal standards of IAA and its metabolites. The pH was adjusted to 2.7 with 1 M hydrochloric acid, and the extracts were purified on Oasis HLB columns (30 mg, Waters Corporation), conditioned with 1 mL methanol, 1 mL water, and 0.5 mL sodium phosphate buffer (pH 2.7). After sample application, the column was washed with 2 mL 5% methanol and then eluted with 2 mL 80% methanol. Eluates were evaporated to dryness and dissolved in 20 μL of mobile phase prior to mass analysis using a 1290 Infinity LC system and 6460 Triple Quad LC-MS system (Agilent Technologies; Novák et al., 2012).

Auxin Accumulation Assays

Assays were performed according to Petrášek et al. (2003). Auxin accumulation was measured in tobacco BY-2 cells (Nagata et al., 1992) 48 h after subcultivation in 0.5 mL aliquots of cell suspension (target working cell density was 7×10^5 cells $\times$ mL^{-1}, and it was determined precisely by counting in the Fuchs-Rosenthal hemocytometer). Cultivation medium was removed by filtration on 20 μm mesh nylon filters, and cells were resuspended in uptake buffer (20 mM MES, 10 mM Suc, 0.5 mM $CaSO_4$, pH adjusted to 5.7 with KOH) and equilibrated for 45 min on the orbital shaker at 27°C in darkness. Equilibrated cells were collected by filtration, resuspended in fresh uptake buffer, and incubated with continuous orbital shaking for another 90 min under the same conditions. Radiolabeled auxin ([^{3}H]NAA or [^{3}H]2,4-D; specific [molar] radioactivity 20 Ci/mmol each; American Radiolabeled Chemicals) was added to the cell suspension to a final concentration of 2 nM. At certain time points, aliquots of the cell suspension were sampled, and accumulation of radiolabeled auxins was terminated by rapid filtration under reduced pressure on cellulose filters (22 mm in diameter). Cell cakes with filters were transferred into scintillation vials, extracted with ethanol (UV-spectroscopy grade) for 30 min, and radioactivity was determined by liquid scintillation counting (Packard Tri-Carb 2900TR scintillation counter, Packard Instrument). Counting efficiency was determined by automatic external standardization, and counts were corrected for quenching automatically. For remaining surface radioactivity, counts were corrected by subtracting counts of aliquots collected immediately after addition of radiolabeled auxin. Inhibitors were added as required from stock solutions to an appropriate final concentration, and proper controls (solvent) were applied. Recorded accumulation values were recalculated to 1 million cells.

Rootward Auxin Transport Assays

Rootward auxin transport assays were performed as described previously (Geisler et al., 2005). In brief, 0.1 μL microdroplets containing 500 nM [^{3}H]IAA (American Radiolabeled Chemicals) and 500 nM cold IAA (Sigma Aldrich) were placed on the shoot apical meristem of Arabidopsis seedlings, and rootward auxin transport was measured by harvesting a 4 mm segment centered on the root shoot transition zone, as well as the entire root, in 2 mm segments (beginning with root zone-1 just after the transition zone, and ending with the main root tip). Treatments with Murashige and Skoog media and 10 μM *c*-CA were carried out by saturating the filter paper matrix on which the roots were incubated during auxin transport assays with Murashige and Skoog media supplemented with either a water:methanol blank or *c*-CA.

Auxin Binding and Anti-auxin Experiments Using SPR and Docking

Auxin receptor proteins AtTIR1 and AtAFB5 were expressed in insect cells (T. ni High5) and purified as described previously (Calderón Villalobos et al., 2012; Lee et al., 2014). The biotinylated degron peptide representing Aux/IAA7 was purchased from ThermoFisher Scientific and immobilized on streptavidin-coated SPR chips (GE Healthcare). SPR experiments were run as described previously (Calderón Villalobos et al., 2012; Lee et al., 2014). Briefly, compounds were added to purified receptor proteins from stock solutions in DMSO to give working concentrations, which were 50 μM unless stated otherwise (DMSO 0.1% final). Controls lacking auxin/compound and controls containing IAA (50 μM) were run as references at the start and end of every set of sensorgrams on every protein preparation. Compounds were run in three separate experiments, with characteristic results shown. For anti-auxin runs, receptor proteins were mixed with 5 μM IAA plus compound at 50 μM. An anti-auxin effect was then determined if the compound competed with IAA, reducing the amplitude of TIR1/AFB5 binding on the sensorgram. Docking was performed using the Vina docking algorithm (Morris et al., 2009; Trott and Olson, 2010). With the TIR1 crystal structure (PDB code 2P1P) from Tan et al. (2007). In silico modeling, molecular graphics, and analyses were performed with the University of California San Francisco Chimera package. Chimera is open source and developed by the Resource for Biocomputing, Visualization, and Informatics at the University of California, San Francisco (supported by NIGMS P41-GM103311; Pettersen et al., 2004). Marvin was used for drawing, displaying, and characterizing chemical structures, substructures, and reactions. Calculator plugins were used for structure property prediction and calculation Marvin v15.10.12.0, 2015, ChemAxon (http://www.chemaxon.com).

Supplemental Figures

The following supplemental materials are available.

Supplemental Figure S1. The general phenylpropanoid pathway.

Supplemental Figure S2. Effect of *c*/*t*-CA on growth and development of different plant species.

Supplemental Figure S3. Photo-isomerization of *c*-CA and *t*-CA.

Supplemental Figure S4. Conversion of *t*-CA by C4H in Arabidopsis.

Supplemental Figure S5. Effect of *c*-CA on *pGATA23*-driven *GUS* expression.

Supplemental Figure S6. Time-dependent *pDR5*-driven *LUC* expression upon *c*-CA treatment.

Supplemental Figure S7. Time-dependent *pDR5*-driven *GFP* expression upon *c*-CA treatment.

Supplemental Figure S8. Docking of *c*-CA and *t*-CA to the auxin binding pocket of TIR1.

Supplemental Figure S9. Shift in IAA-related metabolites upon treatment with 10 μM *c*-CA and *t*-CA for 1 h.

Supplemental Figure S10. Shift in the IAA metabolome upon treatment with 10 μM *c*-CA and *t*-CA for 6 h.

Supplemental Figure S11. The effect on IAA reduction on *c*-CA-mediated developmental defects in seedlings.

Supplemental Figure S12. DII-VENUS response to *c*-CA.

Supplemental Figure S13. DII-VENUS response to NPA.

Supplemental Figure S14. The effect of combined treatment with *c*-CA and NPA on auxin accumulation.

Supplemental Figure S15. The effect of combined treatment with *c*-CA and BUM on auxin accumulation.

Supplemental Figure S16. The effect of *c*-CA on polar auxin transport.

Supplemental Figure S17. Time-dependent *DR5*-driven *LUC* expression upon local application of *c*-CA.

Supplemental Figure S18. The effect of *c*-CA on long distance rootward auxin transport in Arabidopsis.

ACKNOWLEDGMENTS

We thank Ottoline Leyser (Sainsbury Laboratory, University of Cambridge) for providing us *p35S:iaaL* Arabidopsis seeds. We thank Karel Spruyt for imaging wherever needed, Toon Babylon for technical assistance, Wei Xua and Davy

Opdenacker for help with the *pDR5:LUC* experiments, and Tao Fang and Hans Motte for providing us with the *Selaginella moellendorffii* plantlets. We also appreciated the help of the VIB Imaging Core facility, namely Amanda Gonçalves, who helped with analyzing the imaging experiments, and Dominic Petrella for critical reading of the manuscript. Finally, we thank Wim Grunewald, Tom Beeckman, Steffen Vanneste, Bert De Rybel, and Jürgen Kleine-Vehn for scientific discussions.

Received September 29, 2016; accepted November 1, 2016; published November 11, 2016.

LITERATURE CITED

Åberg B (1961) Studies on plant growth regulator XVIII. Some β-substituted acrylic acids. Ann Roy Agric Coll Sweden **27:** 99–123

Adamowski M, Friml J (2015) PIN-dependent auxin transport: action, regulation, and evolution. Plant Cell **27:** 20–32

Beeckman T, Engler G (1994) An easy technique for the clearing of histochemically stained plant tissue. Plant Mol Biol Rep **12:** 37–42

Benková E, Michniewicz M, Sauer M, Teichmann T, Seifertová D, Jürgens G, Friml J (2003) Local, efflux-dependent auxin gradients as a common module for plant organ formation. Cell **115:** 591–602

Blilou I, Xu J, Wildwater M, Willemsen V, Paponov I, Friml J, Heidstra R, Aida M, Palme K, Scheres B (2005) The PIN auxin efflux facilitator network controls growth and patterning in Arabidopsis roots. Nature **433:** 39–44

Boerjan W, Ralph J, Baucher M (2003) Lignin biosynthesis. Annu Rev Plant Biol **54:** 519–546

Brown DE, Rashotte AM, Murphy AS, Normanly J, Tague BW, Peer WA, Taiz L, Muday GK (2001) Flavonoids act as negative regulators of auxin transport in vivo in arabidopsis. Plant Physiol **126:** 524–535

Brunoud G, Wells DM, Oliva M, Larrieu A, Mirabet V, Burrow AH, Beeckman T, Kepinski S, Traas J, Bennett MJ, et al (2012) A novel sensor to map auxin response and distribution at high spatio-temporal resolution. Nature **482:** 103–106

Buer CS, Kordbacheh F, Truong TT, Hocart CH, Djordjevic MA (2013) Alteration of flavonoid accumulation patterns in transparent testa mutants disturbs auxin transport, gravity responses, and imparts long-term effects on root and shoot architecture. Planta **238:** 171–189

Calderón Villalobos LI, Lee S, De Oliveira C, Ivetac A, Brandt W, Armitage L, Sheard LB, Tan X, Parry G, Mao H, et al (2012) A combinatorial TIR1/AFB-Aux/IAA co-receptor system for differential sensing of auxin. Nat Chem Biol **8:** 477–485

Casimiro I, Marchant A, Bhalerao RP, Beeckman T, Shooge S, Swarup R, Graham N, Inzé D, Sandberg G, Casero PJ, Bennet M (2001) Auxin transport promotes Arabidopsis lateral root initiation. Plant Cell **13:** 843–852

Chen YL, Huang ST, Sun FM, Chiang YL, Chiang CJ, Tsai CM, Wang CJ (2011) Transformation of cinnamic acid from trans- to cis-form raises a notable bactericidal and synergistic activity against multiple-drug resistant *Mycobacterium tuberculosis*. Eur J Pharm Sci **43:** 188–194

Colón-Carmona A, You R, Haimovitch-Gal T, Doerner P (1999) Technical advance: spatio-temporal analysis of mitotic activity with a labile cyclin-GUS fusion protein. Plant J **20:** 503–508

De Rybel B, Vassileva V, Parizot B, Demeulenaere M, Grunewald W, Audenaert D, Van Campenhout J, Overvoorde P, Jansen L, Vanneste S, et al (2010) A novel aux/IAA28 signaling cascade activates GATA23-dependent specification of lateral root founder cell identity. Curr Biol **20:** 1697–1706

Delbarre A, Muller P, Imhoff V, Guern J (1996) Comparison of mechanisms controlling uptake and accumulation of 2,4-dichlorophenoxy acetic acid, naphthalene-1-acetic acid, and indole-3-acetic acid in suspension-cultured tobacco cells. Planta **198:** 532–541

Dharmasiri N, Dharmasiri S, Weijers D, Lechner E, Yamada M, Hobbie L, Ehrismann JS, Jürgens G, Estelle M (2005) Plant development is regulated by a family of auxin receptor F box proteins. Dev Cell **9:** 109–119

Ding Z, Galván-Ampudia CS, Demarsy E, Łangowski Ł, Kleine-Vehn J, Fan Y, Morita MT, Tasaka M, Fankhauser C, Offringa R, et al (2011) Light-mediated polarization of the PIN3 auxin transporter for the phototropic response in Arabidopsis. Nat Cell Biol **13:** 447–452

Friml J, Vieten A, Sauer M, Weijers D, Schwarz H, Hamann T, Offringa R, Jürgens G (2003) Efflux-dependent auxin gradients establish the apical-basal axis of Arabidopsis. Nature **426:** 147–153

Fukaki H, Tameda S, Masuda H, Tasaka M (2002) Lateral root formation is blocked by a gain-of-function mutation in the SOLITARY-ROOT/IAA14 gene of Arabidopsis. Plant J **29:** 153–168

Geisler M, Blakeslee JJ, Bouchard R, Lee OR, Vincenzetti V, Bandyopadhyay A, Titapiwatanakum B, Peer WA, Bailly A, Richards EL, et al (2005) Cellular efflux of auxin catalyzed by the Arabidopsis MDR/PGP transporter AtPGP1. Plant J **44:** 179–194

González-Carranza ZH, Elliott KA, Roberts JA (2007) Expression of polygalacturonases and evidence to support their role during cell separation processes in *Arabidopsis thaliana*. J Exp Bot **58:** 3719–3730

Haagen-Smit SAJ, Went FW (1935) A physiological analysis of the growth substance. Proceedings. Koninklijke Akademie van Wetenschappen te Amsterdam **38:** 852–857

Hitchcock AE (1935) Indole-3-n-propionic acid as a growth hormone and quantitative measurement of plant response. *In* Contributions of the Boyce Thompson Institute, **Vol 7**. Boyce Thompson Institute for Plant Research, Yonkers, NY, pp 87–95

Hocking MB (1969) Photochemical and thermal isomerizations of cis- and trans-cinnamic acids, and their photostationary state. Can J Chem **47:** 4567–4576

Kim JY, Henrichs S, Bailly A, Vincenzetti V, Sovero V, Mancuso S, Pollmann S, Kim D, Geisler M, Nam HG (2010) Identification of an ABCB/P-glycoprotein-specific inhibitor of auxin transport by chemical genomics. J Biol Chem **285:** 23309–23317

Kang J, Park J, Choi H, Burla B, Kretzschmar T, Lee Y, Marinoia E (2011) Plant ABC transporters. The Arabidopsis Book **9:** e0153

Koepfli JB, Thimann KB, Went FW (1938) Plant hormones: structure and physiological activity. I. J Biol Chem **122:** 763–780

Kumpf RP, Shi CL, Larrieu A, Stø IM, Butenko MA, Péret B, Riiser ES, Bennett MJ, Aalen RB (2013) Floral organ abscission peptide IDA and its HAE/HSL2 receptors control cell separation during lateral root emergence. Proc Natl Acad Sci USA **110:** 5235–5240

Lee S, Sundaram S, Armitage L, Evans JP, Hawkes T, Kepinski S, Ferro N, Napier RM (2014) Defining binding efficiency and specificity of auxins for SCF(TIR1/AFB)-Aux/IAA co-receptor complex formation. ACS Chem Biol **9:** 673–682

Letham DS (1978) Naturally occurring plant growth regulators other than the principle hormones of higher plants. *In* DS Letham, PB Goodwin, TJV Higgins, eds, Phytohormones and Related Compounds: A Comprehensive Treatise, **Vol 1**. Elsevier/North Holland Biomedical Press, Amsterdam, pp 349–417

Lewis DR, Muday GK (2009) Measurement of auxin transport in *Arabidopsis thaliana*. Nat Protoc **4:** 437–451

Liu C, Xu Z, Chua NH (1993) Auxin polar transport is essential for the establishment of bilateral symmetry during early plant embryogenesis. Plant Cell **5:** 621–630

Lukowitz W, Mayer U, Jürgens G (1996) Cytokinesis in the Arabidopsis embryo involves the syntaxin-related KNOLLE gene product. Cell **84:** 61–71

Moreno-Risueno MA, Van Norman JM, Moreno A, Zhang J, Ahnert SE, Benfey PN (2010) Oscillating gene expression determines competence for periodic Arabidopsis root branching. Science **329:** 1306–1311

Morris GM, Huey R, Lindstrom W, Sanner MF, Belew RK, Goodsell DS, Olson AJ (2009) AutoDock4 and AutoDockTools4: Automated docking with selective receptor flexibility. J Comput Chem **30:** 2785–2791

Nagata T, Nemoto Y, Hasezawa S (1992) Tobacco BY-2 cell-line as the Hela-cell in the cell biology of higher-plants. Int Rev Cytol **132:** 1–30

Novák O, Hényková E, Sairanen I, Kowalczyk M, Pospíšil T, Ljung K (2012) Tissue-specific profiling of the *Arabidopsis thaliana* auxin metabolome. Plant J **72:** 523–536

Okushima Y, Fukaki H, Onoda M, Theologis A, Tasaka M (2007) ARF7 and ARF19 regulate lateral root formation via direct activation of LBD/ASL genes in Arabidopsis. Plant Cell **19:** 118–130

Péret B, De Rybel B, Casimiro I, Benková E, Swarup R, Laplaze L, Beeckman T, Bennett MJ (2009) Arabidopsis lateral root development: an emerging story. Trends Plant Sci **14:** 399–408

Petrášek J, Cerná A, Schwarzerová K, Elckner M, Morris DA, Zazímalová E (2003) Do phytotropins inhibit auxin efflux by impairing vesicle traffic? Plant Physiol **131:** 254–263

Petrášek J, Friml J (2009) Auxin transport routes in plant development. Development **136:** 2675–2688

Petrášek J, Mravec J, Bouchard R, Blakeslee JJ, Abas M, Seifertová D, Wisniewska J, Tadele Z, Kubes M, Covanová M, et al (2006) PIN

proteins perform a rate-limiting function in cellular auxin efflux. Science **312:** 914–918

Pettersen EF, Goddard TD, Huang CC, Couch GS, Greenblatt DM, Meng EC, Ferrin TE (2004) UCSF Chimera—a visualization system for exploratory research and analysis. J Comput Chem **25:** 1605–1612

Romano CP, Hein MB, Klee HJ (1991) Inactivation of auxin in tobacco transformed with the indoleacetic acid-lysine synthetase gene of *Pseudomonas savastanoi*. Genes Dev **5:** 438–446

Santelia D, Henrichs S, Vincenzetti V, Sauer M, Bigler L, Klein M, Bailly A, Lee Y, Friml J, Geisler M, et al (2008) Flavonoids redirect PIN-mediated polar auxin fluxes during root gravitropic responses. J Biol Chem **283:** 31218–31226

Schalk M, Cabello-Hurtado F, Pierrel MA, Atanossova R, Saindrenan P, Werck-Reichhart D (1998) Piperonylic acid, a selective, mechanism-based inactivator of the trans-cinnamate 4-hydroxylase: a new tool to control the flux of metabolites in the phenylpropanoid pathway. Plant Physiol **118:** 209–218

Seifertová D, Skůpa P, Rychtář J, Laňková M, Pařezová M, Dobrev PI, Hoyerová K, Petrášek J, Zažímalová E (2014) Characterization of transmembrane auxin transport in Arabidopsis suspension-cultured cells. J Plant Physiol **171:** 429–437

Tan Z, Calderon-Villalobos LIA, Sharon M, Zheng C, Robinson CV, Estelle M, Zheng N (2007) Mechanism of auxin perception by the TIR1 ubiquitin ligase. Nature **446:** 640–645

Trott O, Olson AJ (2010) AutoDock Vina: improving the speed and accuracy of docking with a new scoring function, efficient optimization, and multithreading. J Comput Chem **31:** 455–461

Van de Wouwer D, Vanholme R, Decou R, Goeminne G, Audenaert D, Nguyen L, Höfer R, Pesquet E, Vanholme B, Boerjan W (2016) Chemical genetics uncovers novel inhibitors of lignification. Plant Physiol **172:** 198–220

Van Overbeek J, Blondeau R, Horne V (1951) Trans-cinnamic acid as an anti-auxin. Am J Bot **38:** 589–595

Vanneste S, Friml J (2009) Auxin: a trigger for change in plant development. Cell **136:** 1005–1016

Vogt T (2010) Phenylpropanoid biosynthesis. Mol Plant **3:** 2–20

Went FW (1939) Analysis and integration of various auxin effects. II. Proceedings. Koninklijke Akademie van Wetenschappen te Amsterdam **42:** 731–739

Wong WS, Guo D, Wang XL, Yin ZQ, Xia B, Li N (2005) Study of cis-cinnamic acid in *Arabidopsis thaliana*. Plant Physiol Biochem **43:** 929–937

Yang XX, Choi HW, Yang SF, Li N (1999) A UV-light activated cinnamic acid isomer regulates plant growth and gravitropism via an ethylene receptor-independent pathway. Aust J Plant Physiol **26:** 325–335

Yin R, Han K, Heller W, Albert A, Dobrev PI, Zažímalová E, Schäffner AR (2014) Kaempferol 3-*O*-rhamnoside-7-*O*-rhamnoside is an endogenous flavonol inhibitor of polar auxin transport in Arabidopsis shoots. New Phytol **201:** 466–475

Yin ZQ, Wong WS, Ye WC, Li N (2003) Biologically active cis-cinnamic acid occurs naturally in *Brassica parachinensis*. Chin Sci Bull **48:** 555–558

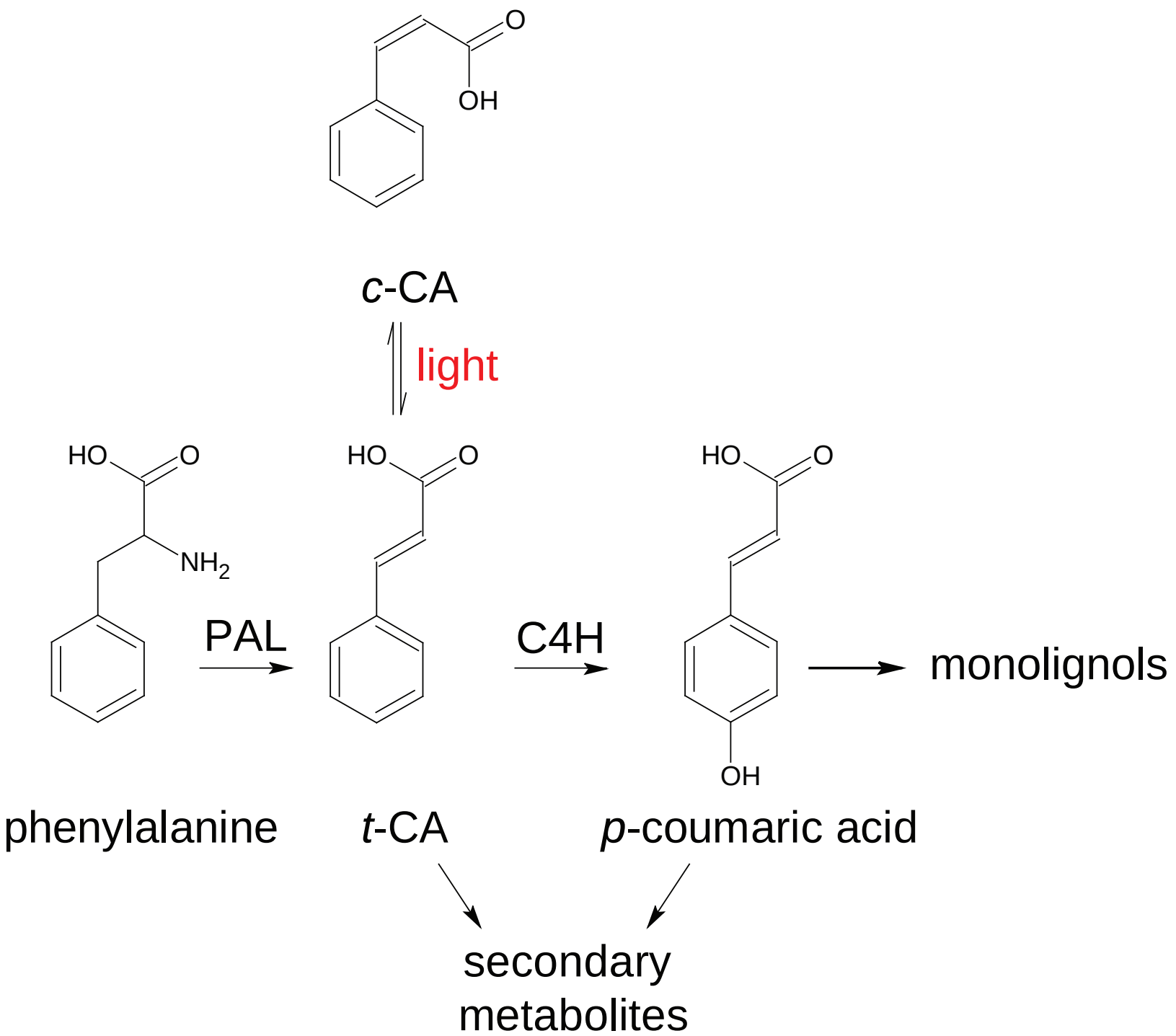

Figure S1. The general phenylpropanoid pathway.

Trans-cinnamic acid (*t*-CA) is synthesized from phenylalanine by PHENYLALANINE AMMONIA-LYASE (PAL) and further hydroxylated to *p*-coumaric acid by CINNAMIC ACID-4-HYDROXYLASE (C4H). These are the first steps of the general phenylpropanoid pathway leading towards a plethora of secondary metabolites, such as flavonoids, stilbenes, tannins and monolignols. *cis*-cinnamic acid (*c*-CA) is a photo-isomerization product of *t*-CA.

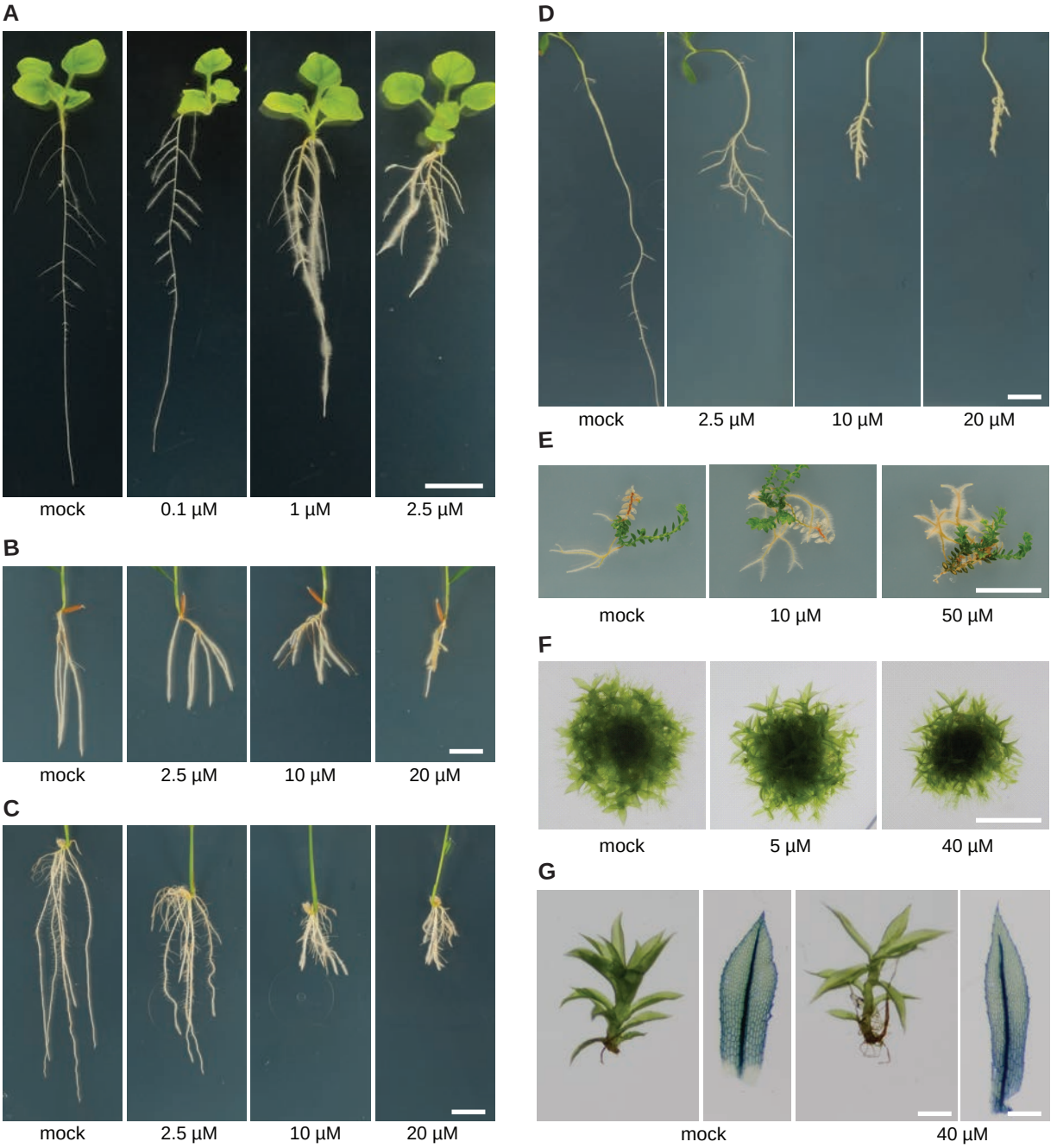

Figure S2. Effect of *c/t*-CA on growth and development of different plant species.

Primary root phenotype of (A) *Nicotiana benthamiana* 14 DAG (n>10), (B) *Brachypodium distachyon* 14 DAG (n>10), (C) *Oryza sativa* 14 DAG (n>10), (D) *Medicago sativa* 14 DAG (n>10) and (E) *Selaginella helvetica* 30 DAG (n>5). (F-G) Leaf phenotype of *Physcomitrella patens* 30 DAG (n>5). All plants were grown on 0.5xMS-medium supplemented with *c/t*-CA. (Scalebar A-F: 1 cm; Scalebar G: 0.1 cm)

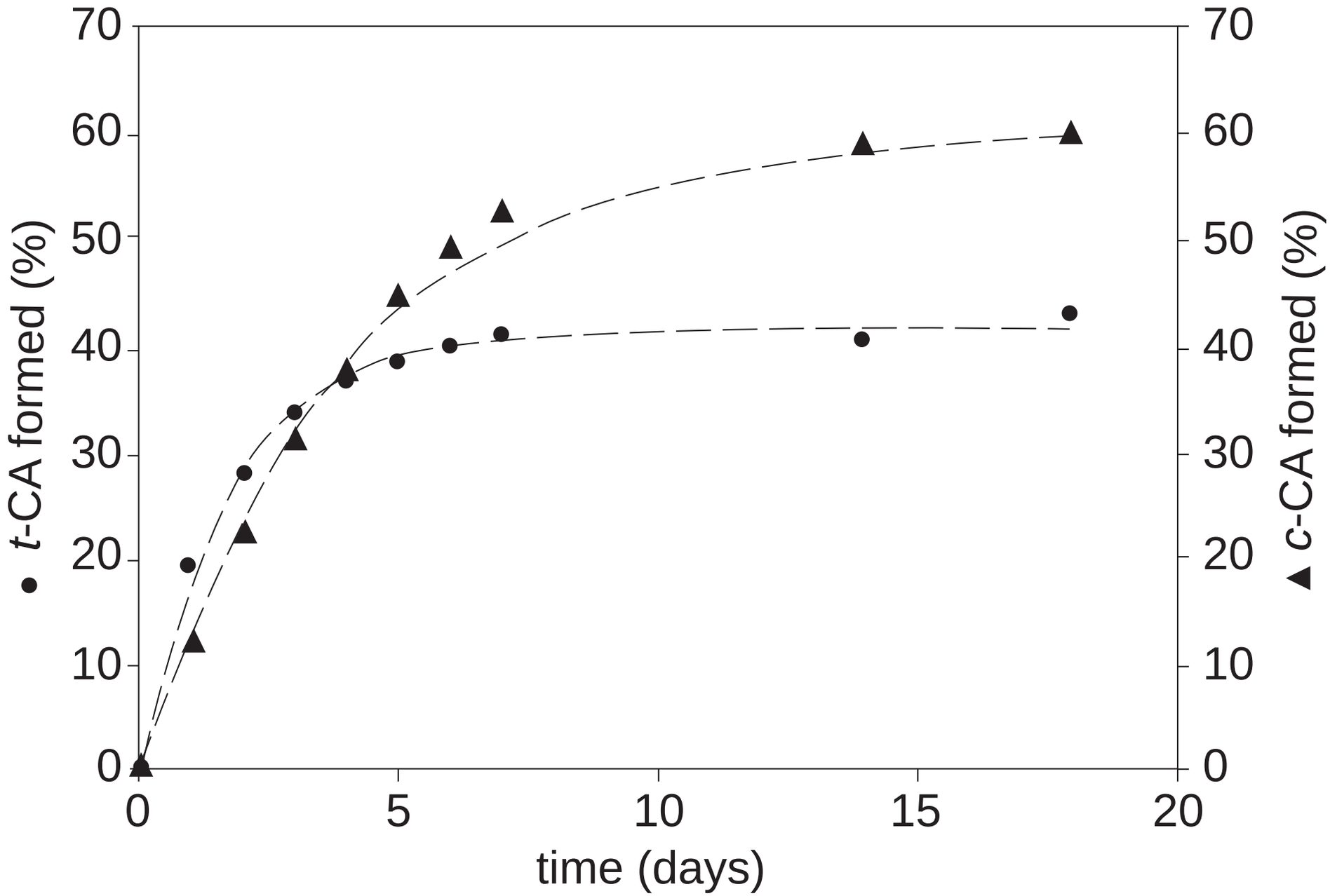

Figure S3. Photo-isomerization of *c*-CA and *t*-CA.

Photo-isomerization of pure *c*-CA or *t*-CA dissolved in Milli-Q-H_2O/DMSO (80/20) and incubated in the growth chamber under a 16h light/8h dark photoperiod. Photo-isomerization was followed on a daily basis for 18 days by UHPLC-MS analysis. A dose response curve was plotted for the conversion of *c*-CA to *t*-CA (dots: exponential decay, single, 3 parameters) and vice versa (triangles: exponential decay, single, 3 parameters).

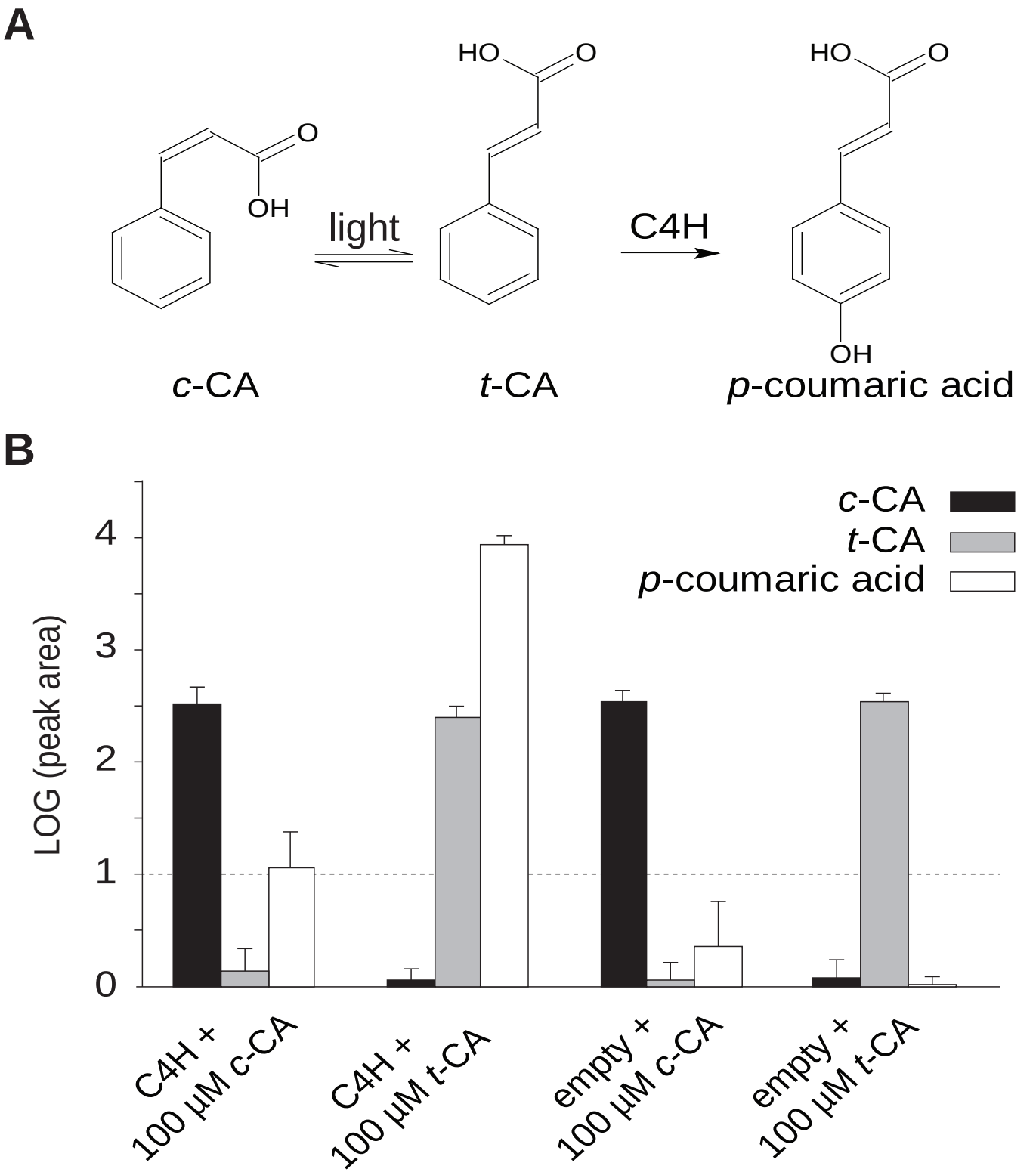

Figure S4. Conversion of *t*-CA by C4H in Arabidopsis.

(A) *t*-CA is hydroxylated to *p*-coumaric acid by CINNAMIC ACID-4-HYDROXYLASE (C4H). *c*-CA is a photo-isomerization product of *t*-CA. (B) Conversion of *c*-CA or *t*-CA towards *p*-coumaric acid using microsomes of yeasts (*Saccharomyces cerevisiae*) expressing *C4H* of Arabidopsis. Both substrate and product were detected by UHPLC-MS analysis (n=6). A treshold (dashed) line was added to the histogram. Error bars represent standard deviations. All proceedings were performed in darkness, and under red-light conditions to make sure no photo-isomerization would occur.

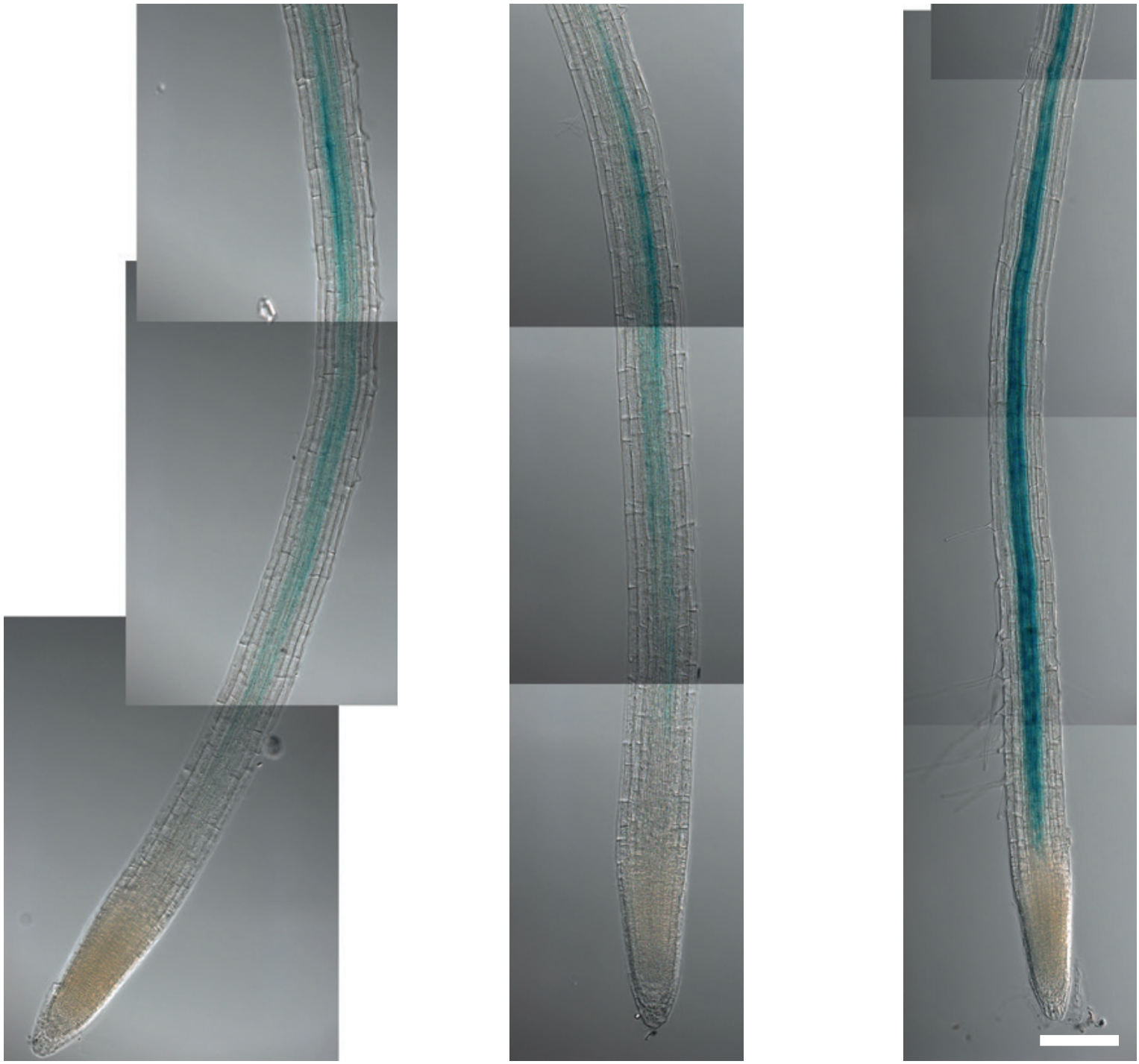

Figure S5. Effect of *c*-CA on GATA23 expression.

Light microscopic images of GATA23 driven GUS expression in the root tip, the zone basal to the main root tip and the elongation zone of GATA23:GUS seedlings 10 DAG. Seed were germinated on 0.5xMS-medium and 7 DAG, seedlings were transferred to 0.5xMS-medium supplemented with 2.5 µM *c*-CA or *t*-CA (n=5) (scale bar: 15 µm).

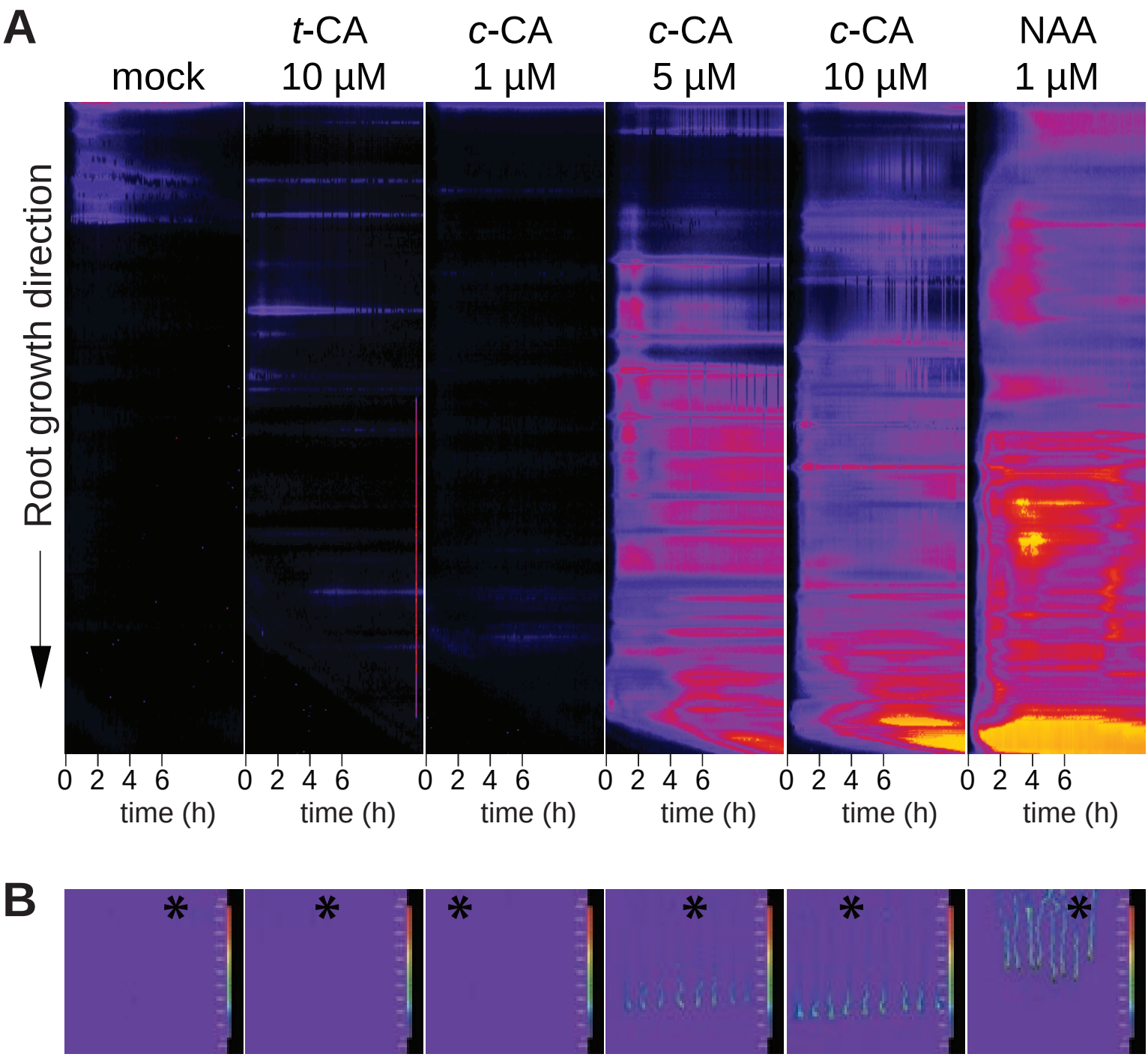

Figure S6. Time dependent *DR5* driven *LUC* expression upon *c*-CA treatment.

(A) Kymograph of *DR5:LUC* intensity along the primary root of Arabidopsis seedlings during a 12h period. The kymograph represents on the vertical axis the primary root, with the root tip present in the orignin of the coordinate system, and the shoot/root junction at the end of the vertical axis. The horizontal axis represents time. Seeds were germinated on 0.5xMS-medium and 5 DAG seedlings were transferred to 0.5xMS-medium supplemented with 1-10 µM *c*-CA, 10 µM *t*-CA or 1 µM NAA. Imaging was started at the moment of transfer and done every 10 minutes. Each kymograph represents one experiment. The kymograph is representative for 8 biological repeats (seedlings). (B) Images of the final *LUC* intensity expression at the end of the experiment described in (A). Asterisks indicate the selected seedling for creation of the kymograph.

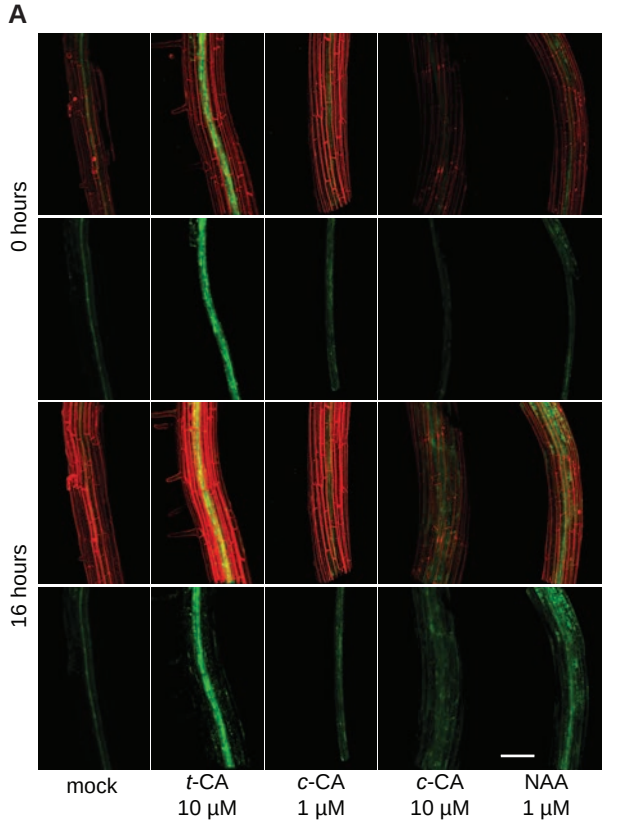

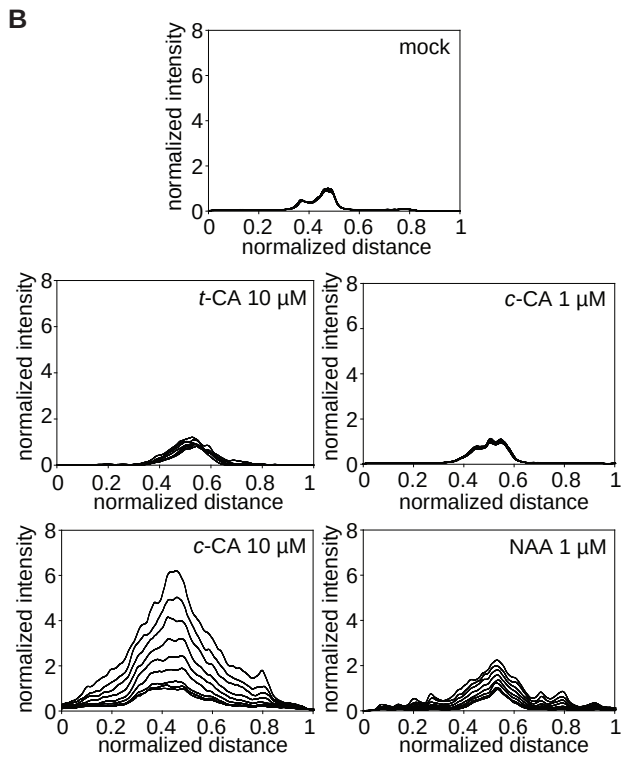

Figure S7. Time dependent *DR5* driven *GFP* expression upon *c*-CA treatment.

Confocal time-lapse imaging of *DR5rev:GFP* intensity in the primary root between two young emerged lateral roots. Seedlings were placed in glass-bottomed chambers and covered with 0.5xMS-media containing 1 µM NAA, 1-10 µM *c*-CA or 10 µM *t*-CA. Time-lapse was started 5 minutes after the seedlings had been placed in contact with the media and images were captured every 60 minutes over a 16h period. (A) Z-projection of the *DR5rev:GFP* intensity at the onset of the experiment and the end of the experiment (16 hours). (B) Cumulative spectrum obtained by projecting the *GFP* intensity on a virtual line crossing the middle of the primary root. Normalization was performed against the maximal intensity of the signal at the earliest time point (n=1). Each spectrum is representative for 3 biological repeats (positions along the primary root).

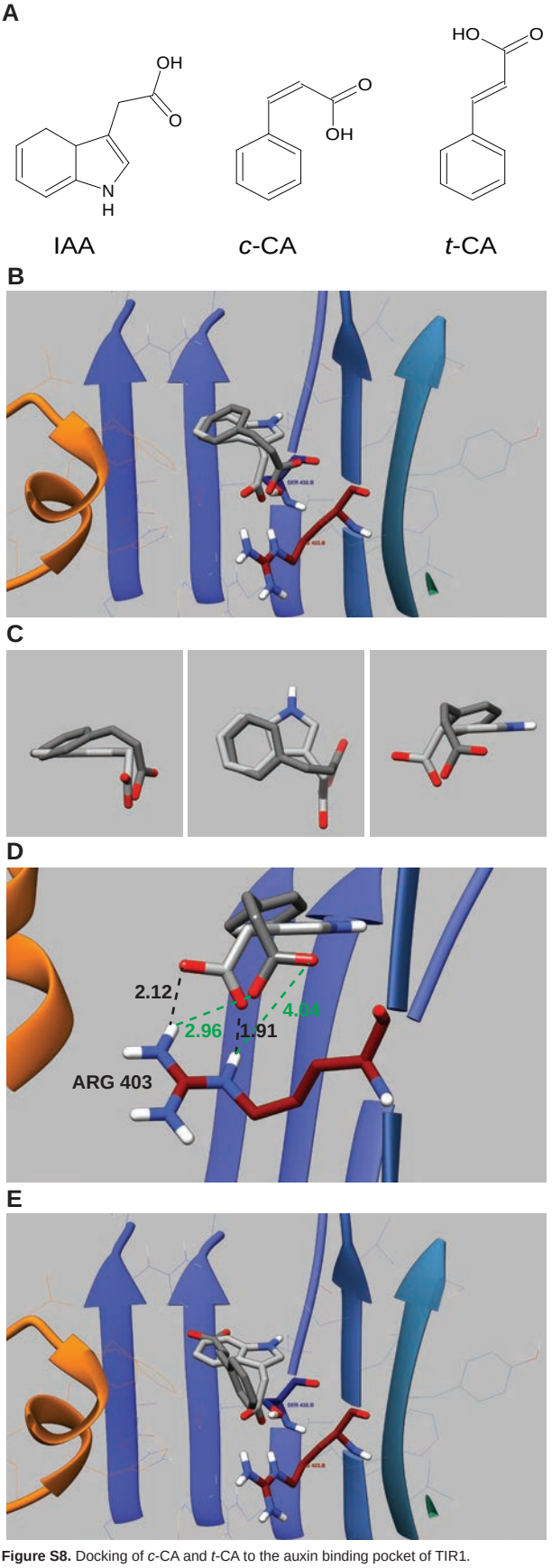

Figure S8. Docking of *c*-CA and *t*-CA to the auxin binding pocket of TIR1.

(A) The molecular structure of IAA, *c*-CA and *t*-CA. (B) The best possible pose for *c*-CA in the lower region of the TIR1 pocket. (C) Different perspectives of view of *c*-CA with respect to IAA for binding with the TIR1 pocket. (D) Close-up of the best possible pose for *c*-CA in the lower region of the TIR1 pocket. (E) The best possible pose for *t*-CA in the lower region of the TIR1 pocket.

Indole-3-acetic acid, precursors, conjugates and catabolites levels (pg/mg fresh weight) (1 hour incubation)

	mock	***c*-CA 10 µM**	***t*-CA 10 µM**
indole-3-acetic acid	12.13 ± 2.14	14.02 ± 2.11	14.21 ± 1.83
precursors			
anthranilate	21.98 ± 4.69	23.52 ± 4.39	26.51 ± 4.92
L-tryptophan	4592.4 ± 966.3	4848.5 ± 646.7	4771.5 ± 765.6
tryptamine	0.27 ± 0.05	0.34 ± 0.01	0.38 ± 0.07
indole-3-acetamide	0.87 ± 0.23	1.25 ± 0.26	1.16 ± 0.28
indole-3-acetonitrile	77660.0 ± 15162.2	129092.8 ± 34300.5	124503.4 ± 31905.2
indole-3-acetaldoxime	8.21 ± 1.87	13.48 ± 3.40	8.23 ± 0.54
indole-3-acetaldehyde	60.1 ± 11.3	74.1 ± 11.6	61.7 ± 8.2
indole-3-pyruvic acid	65.67 ± 10.47	79.93 ± 14.25	71.51 ± 11.29
catabolites, conjugates:			
2-oxindole-3-acetic acid	37.12 ± 6.60	57.05 ± 10.09 *	59.98 ± 8.39 *
IAA-glutamate	1.15 ± 0.19	1.32 ± 0.27	1.68 ± 0.39
IAA-aspartate	0.9 ± 0.2	1.1 ± 0.3	1.4 ± 0.4

Figure S9. Shift in IAA related metabolites upon treatment with 10 µM *c*-CA and *t*-CA for 1h.

The concentration of free IAA, IAA-precursors, IAA-amino acid conjugates and IAA-degradation products in 12 DAG Arabidopsis seedlings grown on 0.5xMS-medium and transferred for 1 hour to 0.5xMS-medium supplemented with 10 µM *c*-CA or *t*-CA. To avoid isomerization of the CA, the incubation was performed in darkness. Ten seedlings were pooled for each technical repeat, and four repeats were analyzed for each treatment. Error bars represent standard deviations and asterisks statistically significant differences between compound-treated and mock-treated plants as determined by Dunnett's test. P-values: *P < 0.05, **P < 0.001, *** P <0.0001.

Indole-3-acetic acid, precursors, conjugates and catabolites levels (pg/mg fresh weight) (6 hours incubation)

	mock	***c*-CA 10 µM**		***t*-CA 10 µM**
indole-3-acetic acid	10.61 ± 1.97	13.09 ± 1.27		10.78 ± 2.68
precursors:				
anthranilate	18.08 ± 2.89	17.38 ± 2.84		16.74 ± 3.97
L-tryptophan	6565.2 ± 819.5	6742.5 ± 881.1		5777.4 ± 1110.3
tryptamine	0.27 ± 0.07	0.21 ± 0.05		0.23 ± 0.03
indole-3-acetamide	0.58 ± 0.10	0.91 ± 0.18	*	0.61 ± 0.15
indole-3-acetonitrile	47028.1 ± 11186.1	101519.9 ± 26153.6	*	78439.3 ± 22573.0
indole-3-acetaldoxime	4.83 ± 0.75	10.57 ± 2.23	*	5.04 ± 1.10
indole-3-acetaldehyde	67.6 ±14.9	121.4 ± 23.9	*	95.8 ± 22.7
indole-3-pyruvic acid	73.04 ± 17.30	131.60 ± 8.94	**	88.98 ± 21.48
catabolites, conjugates:				
2-oxindole-3-acetic acid	35.04 ± 9.22	46.08 ± 4.02		38.76 ± 11.43
IAA-glutamate	1.28 ± 0.27	1.49 ± 0.29		1.30 ± 0.12
IAA-aspartate	1.7 ± 0.5	2.2 ± 0.6		1.6 ± 0.3

Figure S10. Shift in the IAA metabolome upon treatment with 10 µM *c*-CA and *t*-CA for 6h.

The concentration of free IAA, IAA-precursors, IAA-amino acid conjugates and IAA-degradation products in 12 DAG Arabidopsis seedlings grown on 0.5xMS-medium and transferred for 6 hours to 0.5xMS-medium supplemented with 10 µM *c*-CA or *t*-CA. To avoid isomerization of the CA, the incubation was performed in darkness. Ten seedlings were pooled for each technical repeat, and four repeats were analyzed for each treatment. Error bars represent standard deviations and asterisks statistically significant differences between compound-treated and mock-treated plants as determined by Dunnett's test. P-values: *P < 0.05, **P < 0.001, *** P <0.0001.

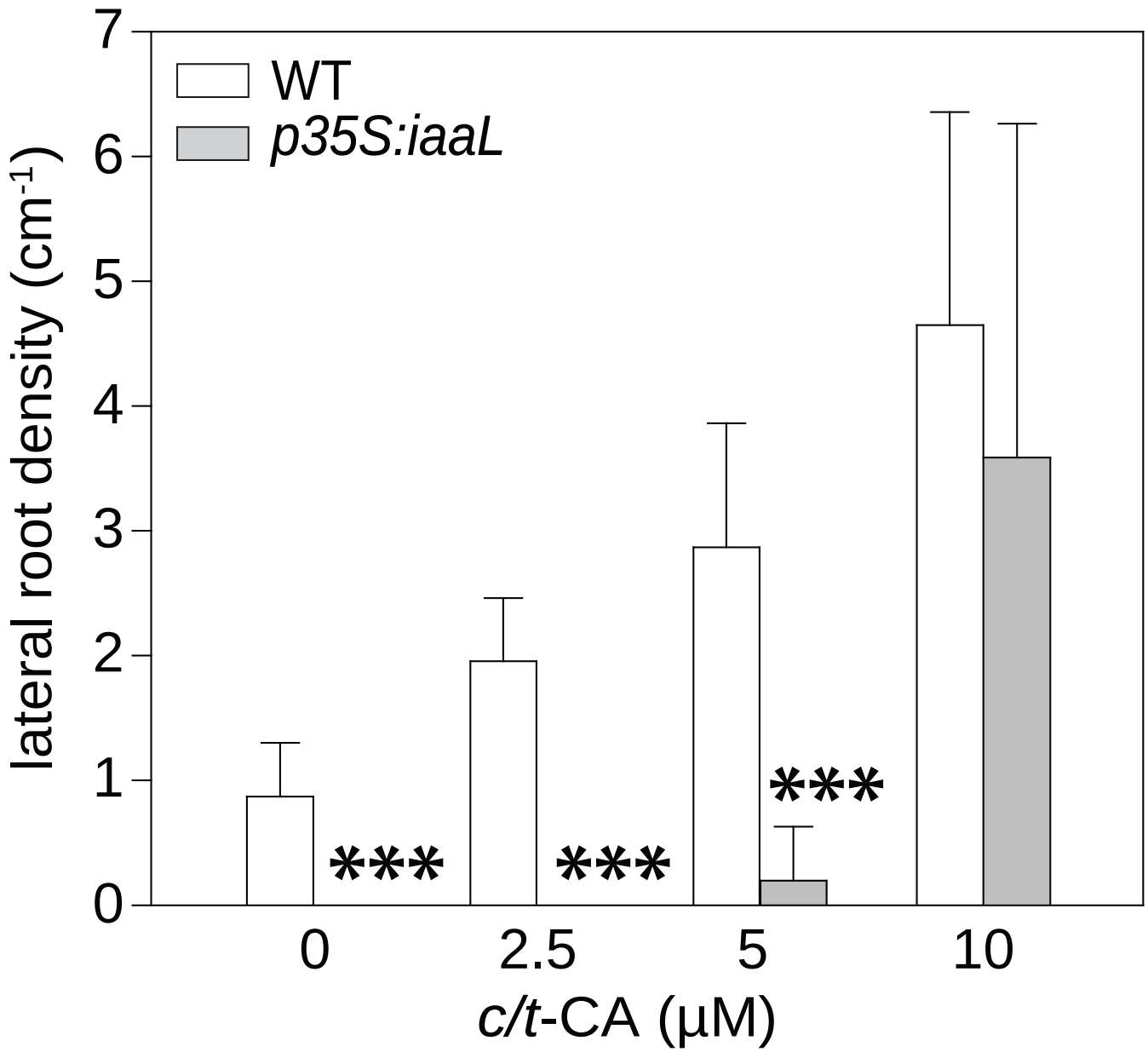

Figure S11. The effect on IAA reduction on *c*-CA mediated developmental defects in seedlings.

Lateral root density of WT and *p35S:iaaL* seedlings 10 DAG grown on 0.5xMS-medium, supplemented with different concentrations of *c/t*-CA (n>20 for each concentration). Error bars represent standard deviations and asterisks represent statistically significant differences between WT and *p35S:iaaL* at each concentration as determined by Dunnett's test P-values: *P < 0.05, **P < 0.001, *** P <0.0001.

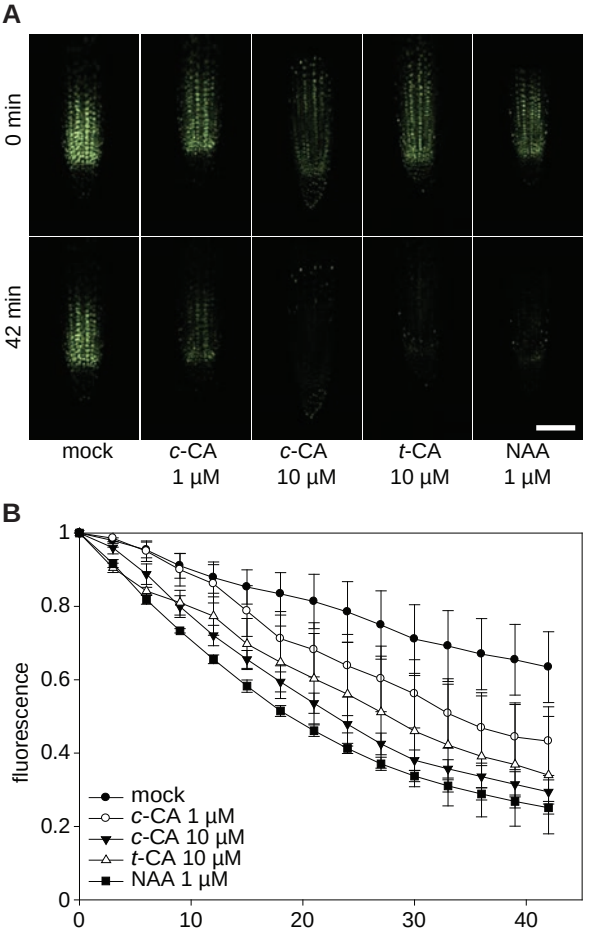

Figure S12. DII-VENUS response to *c*-CA.

(A) Confocal images of DII-VENUS degradation in the main root tip of *DII-VENUS-YFP* seedlings. Plants were germinated on 0.5xMS-medium and subsequently transferred 5 DAG to 0.5xMS-medium supplemented with 1 or 10 µM *c*-CA, 10 µM *t*-CA or 1 µM 1-NAA. Individual root tips were imaged at the onset of the experiment and after 42 minutes (n=3) (scale bar: 50 µm). (B) Time-course of DII-VENUS fluorescence in the main root tip of plants grown as described above. Fluorescence was quantified every 3 minutes over a 42 minute period. During each experiment 3 root tips (representing one treatment) were simultaneously imaged. Error bars represent standard deviations.

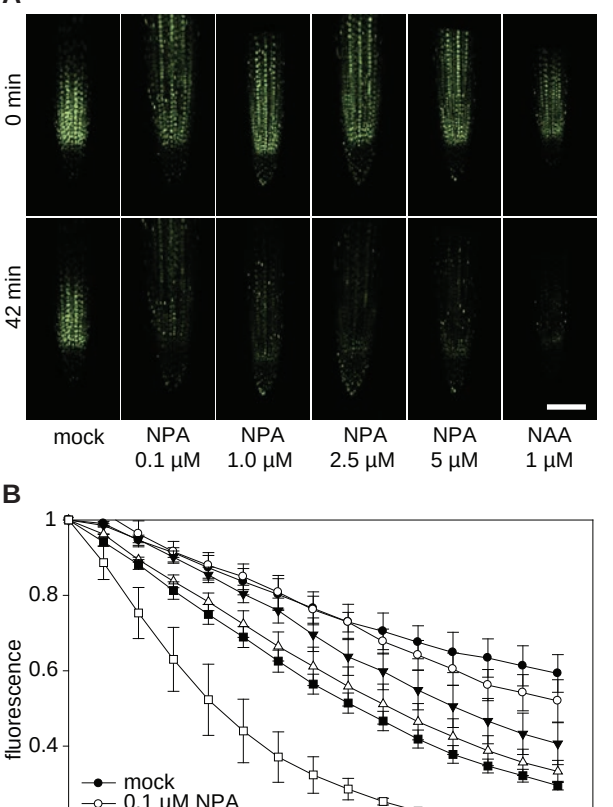

Figure S13. DII-VENUS response to NPA.

(A) Confocal images of DII-VENUS degradation in the main root tip of *DII-VENUS-YFP* seedlings. Plants were germinated on 0.5xMS-medium and subsequently transferred 5 DAG to 0.5xMS-medium supplemented with 0.1-5 µM NPA or 1 µM 1-NAA. Individual root tips were imaged at the onset of the experiment and after 42 minutes (n=3) (scale bar: 50 µm). (B) Time-course of DII-VENUS fluorescence in the main root tip of plants grown as described above. Fluorescence was quantified every 3 minutes over a 42 minute period. During each experiment 3 root tips (representing one treatment) were simultaneously imaged. Error bars represent standard deviations.

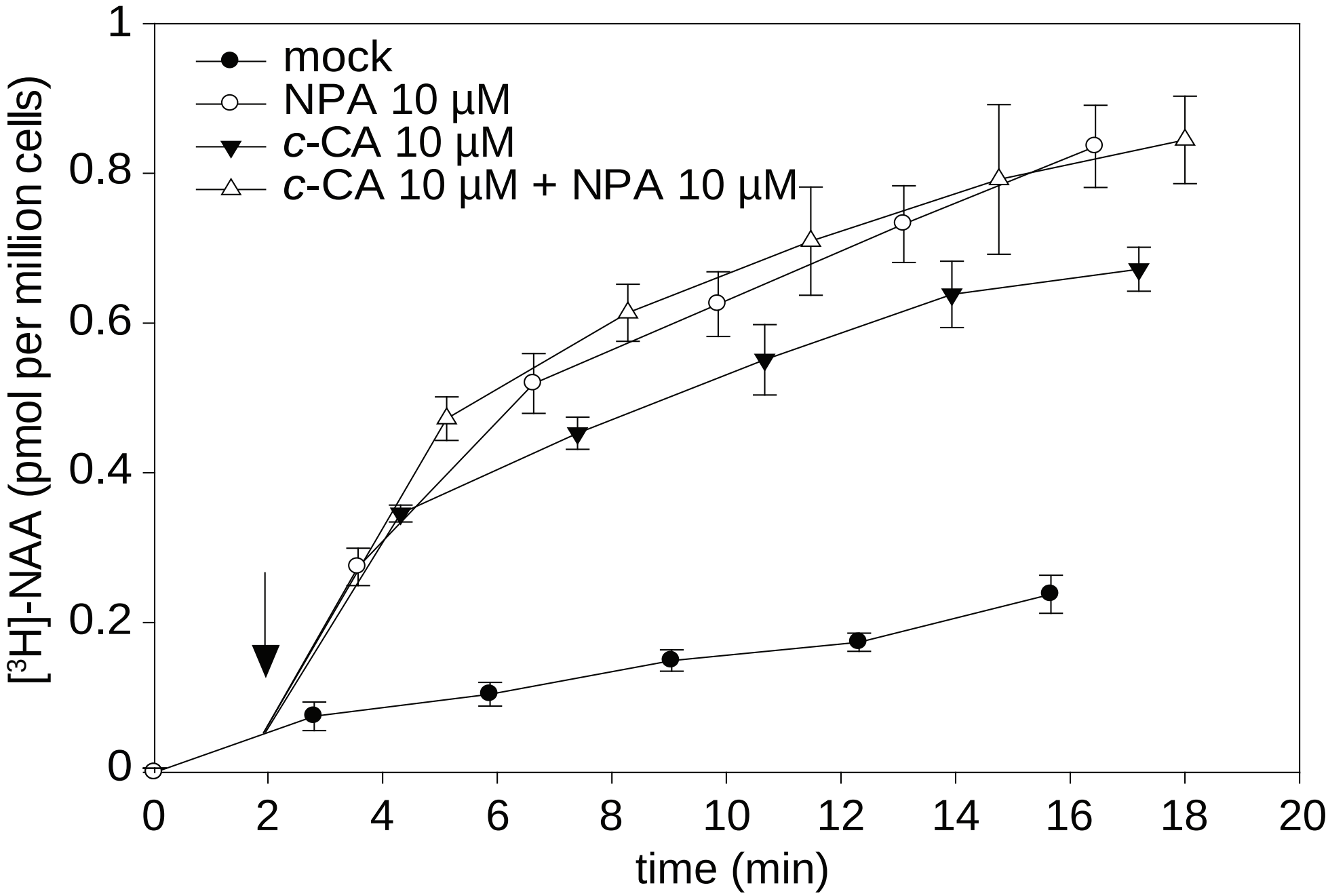

Figure S14. The effect of combined treatment with *c*-CA and NPA on auxin accumulation.

The combined effect of 10 µM c-CA and NPA on the net accumulation of [^{3}H]-NAA in 2-days old suspension-cultured tobacco BY-2 cells. The arrow points to the time of application of the compounds. Error bars represent standard deviations (n=4).

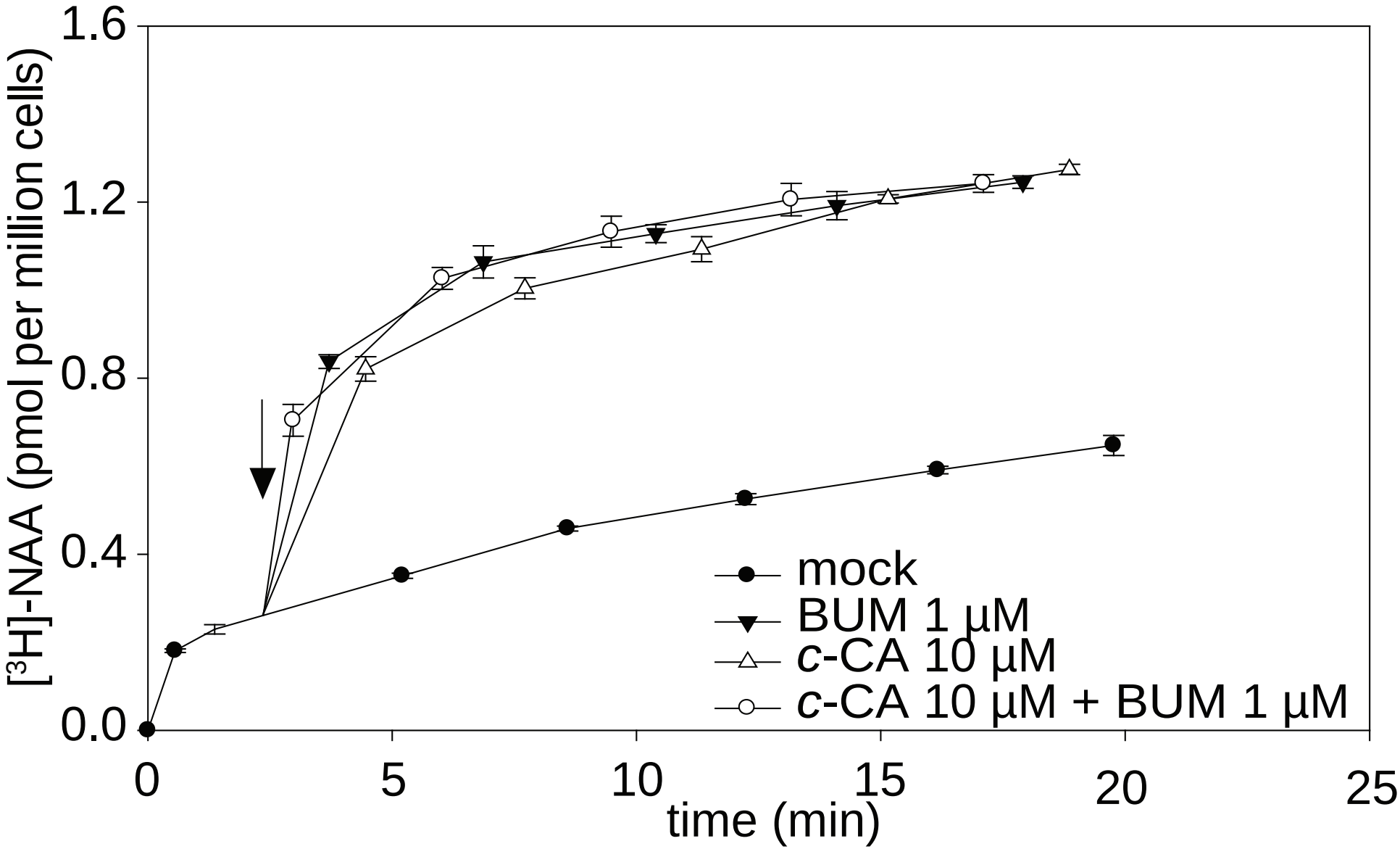

Figure S15. The effect of combined treatment with *c*-CA and BUM on auxin accumulation.

The combined effect of 10 µM *c*-CA and 1 µM BUM on the net accumulation of [^{3}H]-NAA in 2-days old suspension-cultured tobacco BY-2 cells. The arrow points to the time of application of the compounds. Error bars represent standard deviations (n=4).

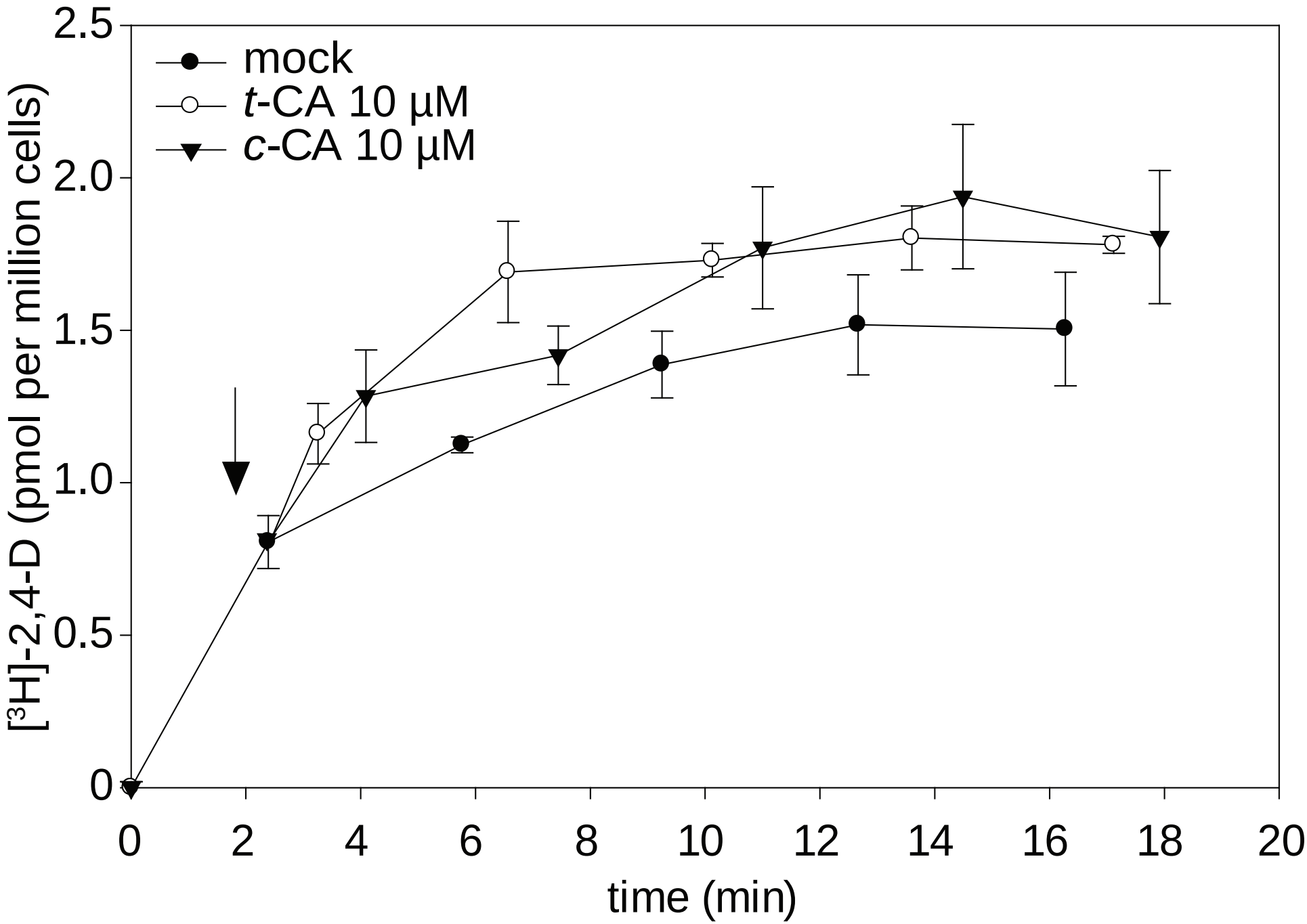

Figure S16. The effect of *c*-CA on polar auxin transport

Effect of 10 µM *c*-CA or 10 µM *t*-CA on the net accumulation of [^{3}H]-2,4-D in 2-day old suspension-cultured tobacco BY-2 cells. The arrows points to the time of application of the compound. Error bars represent standard deviations (n=4).

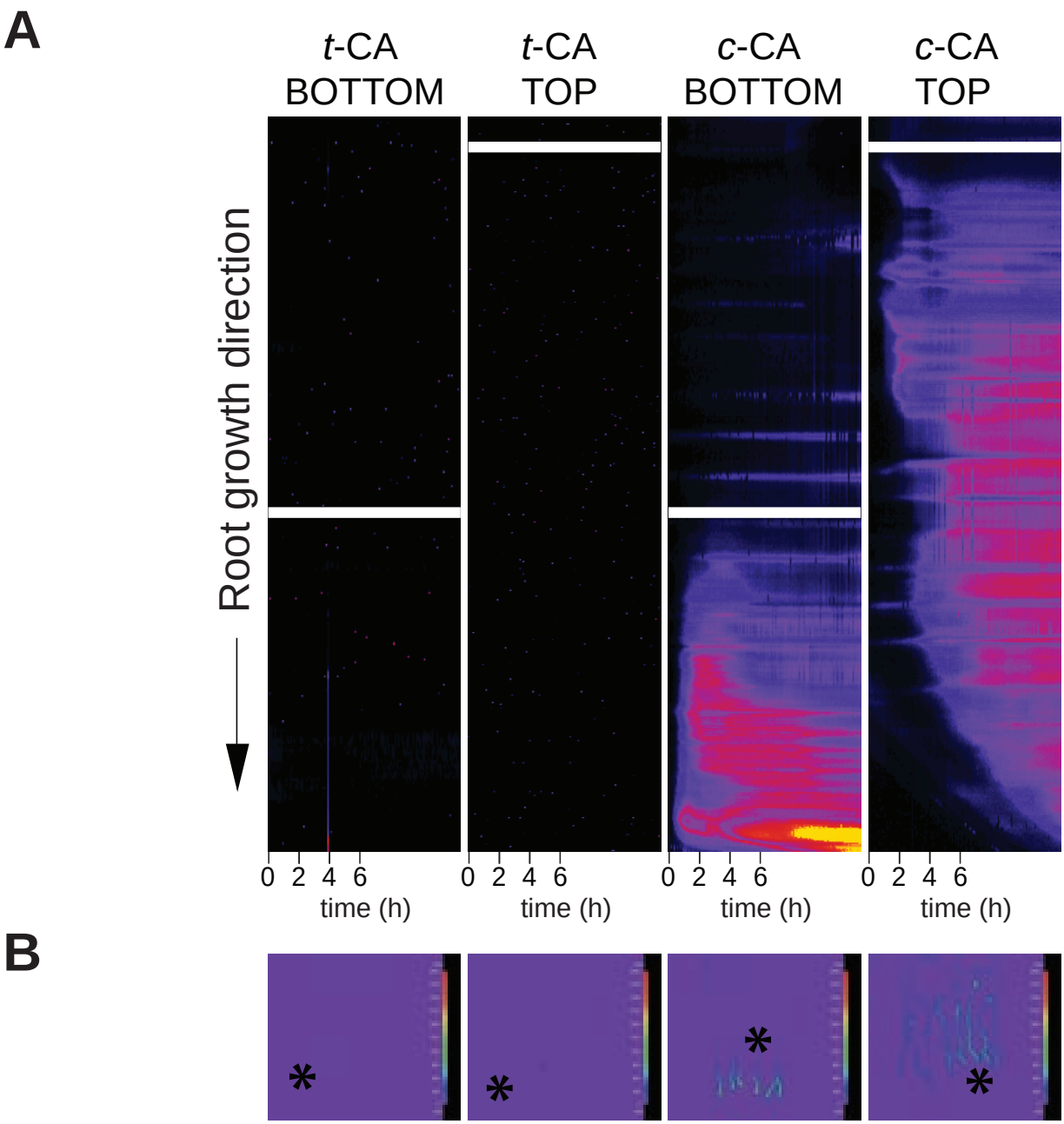

Figure S17. Time dependent *DR5* driven *LUC* expression upon local application of *c*-CA.

(A) Kymograph of *DR5:LUC* intensity along the primary root of Arabidopsis seedlings during a 12h period. The kymograph represents on the vertical axis the primary root, with the root tip present in the origin of the coordinate system, and the shoot/root junction at the end of the vertical axis. The horizontal axis represents time. Seeds were germinated on 0.5xMS-medium and 5 DAG seedlings were transferred to 0.5xMS-medium supplemented with 10 µM *c*-CA or *t*-CA. The compound of interest was locally applied to the 0.5xMS-medium, visualized by the full white line in the kymograph that seperates the mock-treated medium from the compound-treated one. Imaging was inititated the moment of transfer and done every 10 minutes. Each kymograph represents one experiment. The kymograph is representative for more than 6 biological repeats (seedlings). (B) Images of the final *LUC* intensity at the end of the experiment described in (A). Asterisks indicate the selected seedling for creation of the kymograph.

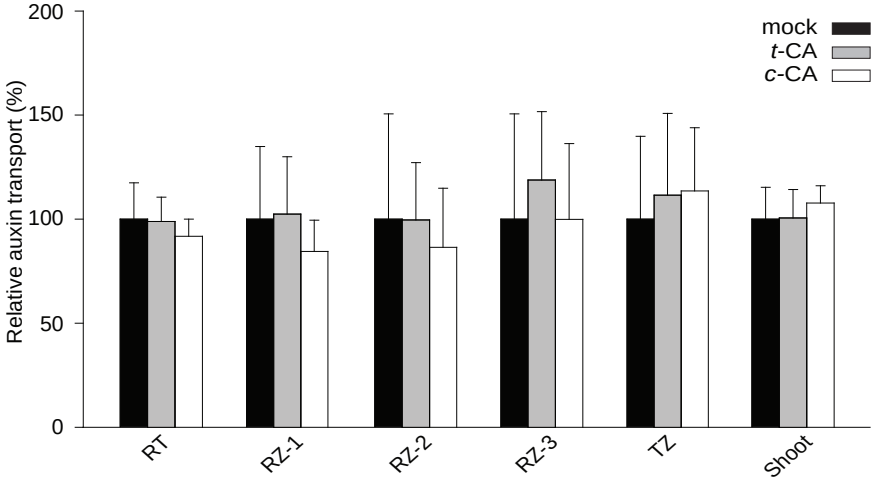

Figure S18. The effect of *c*-CA on long distance rootward auxin transport in Arabidopsis.

Rootward long distance [^{3}H]-IAA transport from the shoot apical meristem in 5 day old WT seedlings pre-treated for 2 hours with 10 µM *c*-CA or *t*-CA. Rootward auxin transport was measured 5 hours after locally applying a microdroplet of [^{3}H]-IAA to the shoot apical meristem and by harvesting a 4 mm segment centered on the root shoot transition zone (TZ), as well as the entire root, in 2 mm segments (beginning with root zone-(RZ)-1 just after the TZ, and ending with the root tip (RT)) (n=3). Error bars represent standard deviations and asterisks were used to indicate statistically significant differences compared to the corresponding mock-treated control sample as determined by Dunnett's test P-values: *P < 0.05, **P < 0.001, *** P <0.0001.